


Politecnico di Torino

Micro and Nanotechnologies for Integrated Systems

Bulk and Surface modifications for Wide Bandgap Perovskite Solar Cells

Supervisors:

Cristian Villalobos Meza
Dr. Yinghuan Kuang
Prof. Federica Cappelluti

Candidate:

Marialucia D'Addio

Academic year 2023/2024

To those who were forced to leave,
And to those who chose to stay.

Abstract

The accelerating impact of climate change and global pollution has led to a rapidly increasing demand for renewable energy sources. Among these, photovoltaic energy has emerged as a leading candidate for achieving sustainability and energy efficiency. However, the development of efficient and stable wide bandgap perovskite materials for use in silicon-perovskite tandem solar cells for even higher power output remains a significant challenge. These materials are critical because defects in the perovskite bulk and at interfaces can increase charge carrier recombination, thereby limiting device performance.

This research addresses this challenge by optimizing the wide bandgap perovskite optoelectrical properties via bulk and interfacial modulation. The wide bandgap halide perovskites were fabricated via a vapor-solution hybrid approach. Bulk additives and surface passivating materials are investigated to enhance the perovskite quality and eventually device performance. Additionally, a morphology study was conducted on silicon cells to better understand deposition conditions of perovskite layer stack on textured silicon substrates, with the goal of applying these insights to develop more efficient perovskite/silicon two-terminal tandem solar cells.

For characterization, scanning electron microscopy was employed to analyze sample morphology, while a solar simulator provided figures of merit for the solar cells. Photoluminescence measurements further elucidated the bandgap properties of the materials.

19% efficiency was obtained for inverted p-i-n 1.67 eV perovskite solar cells based on a fully scalable cell architecture.

The incorporation of additive materials and interlayers showed considerable potential in enhancing device efficiency and overall performance. However, further research is necessary to fully understand the underlying mechanisms and optimize these additives for broader application. Future work will focus on refining these techniques, determining optimal additive concentrations, and conducting additional characterization to achieve reproducible enhancement in device performance.

Sommario

Gli effetti accelerati del cambiamento climatico e dell'inquinamento globale hanno portato a un aumento rapido della domanda di energie rinnovabili. Tra queste, l'energia fotovoltaica è diventata una delle soluzioni principali per raggiungere la sostenibilità e migliorare l'efficienza energetica. Tuttavia, lo sviluppo di materiali perovskitici stabili ed efficienti a larga banda proibita, da impiegare nelle celle solari tandem silicio-perovskite per ottenere una maggiore potenza di uscita, rimane una sfida significativa. Questi materiali sono cruciali poiché i difetti nel bulk della perovskite e alle interfacce possono aumentare la ricombinazione dei portatori di carica, riducendo così le prestazioni del dispositivo.

Questa ricerca si concentra sull'ottimizzazione delle proprietà optoelettroniche della perovskite a larga banda proibita, agendo sia a livello del bulk che delle interfacce. Le perovskiti alogenate a larga banda proibita sono state prodotte tramite un approccio ibrido vapore-soluzione. Additivi nel bulk e materiali passivanti di superficie sono stati studiati per migliorare la qualità della perovskite e, di conseguenza, le prestazioni del dispositivo. È stato inoltre condotto uno studio morfologico su celle di silicio per comprendere meglio le condizioni di deposizione dello stack di strati di perovskite su substrati di silicio testurizzati, con l'obiettivo di applicare queste conoscenze per sviluppare celle tandem perovskite/silicio a due terminali più efficienti.

La caratterizzazione è stata eseguita utilizzando la microscopia elettronica a scansione per analizzare la morfologia dei campioni, mentre un simulatore solare ha fornito le figure di merito delle celle. Le misurazioni di fotoluminescenza hanno ulteriormente chiarito le proprietà di banda proibita dei materiali.

È stata raggiunta un'efficienza del 19% per celle solari invertite p-i-n in perovskite da 1,67 eV, basate su un'architettura di cella completamente scalabile.

L'incorporazione di additivi e strati intermedi ha mostrato un notevole potenziale per migliorare l'efficienza e le prestazioni complessive dei dispositivi. Tuttavia, sono necessarie ulteriori ricerche per comprendere meglio i meccanismi sottostanti e ottimizzare questi additivi per un'applicazione più ampia. I lavori futuri si concentreranno sul perfezionamento di queste tecniche, sulla determinazione delle concentrazioni ottimali degli additivi e su ulteriori caratterizzazioni per ottenere un miglioramento riproducibile delle prestazioni.

Résumé

L'accélération de l'impact du changement climatique et de la pollution mondiale a entraîné une augmentation rapide de la demande en sources d'énergie renouvelables. Parmi celles-ci, l'énergie photovoltaïque s'est imposée comme un candidat de choix pour atteindre la durabilité et l'efficacité énergétique. Toutefois, le développement de matériaux pérovskites à large bande interdite efficaces et stables, destinés à être utilisés dans des cellules solaires tandem silicium-pérovskite pour une puissance de sortie encore plus élevée, reste un défi de taille. Ces matériaux sont essentiels car les défauts dans la pérovskite et aux interfaces peuvent augmenter la recombinaison des porteurs de charge, limitant ainsi les performances de l'appareil.

Cette recherche relève ce défi en optimisant les propriétés optoélectriques de la pérovskite à large bande interdite par le biais d'une modulation globale et interfaciale. Les pérovskites d'halogénure à large bande interdite ont été fabriquées par une approche hybride vapeur-solution. Des additifs en vrac et des matériaux de passivation de surface ont été étudiés pour améliorer la qualité de la pérovskite et, ainsi, la performance du dispositif. En outre, une étude morphologique a été menée sur des cellules de silicium afin de mieux comprendre les conditions de dépôt de l'empilement de couches de pérovskite sur des substrats de silicium texturés, dans le but d'appliquer ces connaissances pour développer des cellules solaires tandem pérovskite/silicium à deux terminaux plus efficaces.

Pour la caractérisation, la microscopie électronique à balayage a été utilisée pour analyser la morphologie des échantillons, tandis qu'un simulateur solaire a fourni des données de performance pour les cellules solaires. Les mesures de photoluminescence ont permis d'élucider les propriétés de la bande interdite des matériaux.

Un rendement de 19% a été obtenu pour les cellules solaires p-i-n inversées en pérovskite à 1,67 eV basées sur une architecture de cellule entièrement évolutive.

L'incorporation de matériaux additifs et de couches intermédiaires a montré un potentiel considérable dans l'amélioration de l'efficacité du dispositif et de la performance globale. Toutefois, des recherches supplémentaires sont nécessaires pour comprendre pleinement les mécanismes sous-jacents et optimiser ces additifs en vue d'une application plus large. Les travaux futurs se concentreront sur le perfectionnement de ces techniques, la détermination des concentrations optimales d'additifs et la réalisation de caractérisations supplémentaires afin d'obtenir une amélioration reproductible des performances des dispositifs.

Contents

1 Green energy transition and photovoltaics **6**
- 1.1 Photovoltaics on the market . . . 6
- 1.2 Solar spectrum and Air mass . . . 6
- 1.3 Basic working principles of solar cells . . . 8
- 1.4 Quantifying Solar Cell Performance:Figures of Merit . . . 9
- 1.5 Silicon solar cells . . . 11
  - 1.5.1 Shockley-Queisser limit . . . 12
- 1.6 Multi-junction solar cells . . . 12
- 1.7 Thin film solar cells and emerging materials . . . 12

2 Perovskite-based single and multi-junction solar cells **14**
- 2.1 Perovskite chemical structure . . . 15
- 2.2 Perovskite Absorber Layer . . . 15
  - 2.2.1 Perovskite-Silicon tandem solar cells . . . 16
- 2.3 Fabrication of perovskite single-junction cells . . . 17
  - 2.3.1 Hole Transport Layer . . . 17
  - 2.3.2 Perovskite absorber layer . . . 21
  - 2.3.3 Electron transport layer . . . 22
  - 2.3.4 Metal contacts . . . 23
  - 2.3.5 Semitransparent single-junction solar cell . . . 24
- 2.4 Fabrication of tandem cells . . . 24
- 2.5 Characterization . . . 25
  - 2.5.1 Solar Simulator . . . 25
  - 2.5.2 SEM . . . 26
  - 2.5.3 Photoluminescence . . . 26

3 Wide bandgap perovskite solar cell development by vapor-solution hybrid approach **28**
- 3.1 Silicon Heterojunctions Cells – Effect of Annealing Temperature . . . 28
- 3.2 Reflection in Silicon Solar Cells . . . 29
- 3.3 Morphology study . . . 30
- 3.4 Adjusting the organic solution composition . . . 34
- 3.5 Bulk and surface modification . . . 37
  - 3.5.1 Bulk modification . . . 37
  - 3.5.2 Surface modification . . . 43
- 3.6 Conclusion . . . 47

4 Conclusion and Outlook **48**

Chapter 1

Green energy transition and photovoltaics

1.1 Photovoltaics on the market

According to the 2023 International Energy Agency (IEA) report on renewable energy, global annual renewable capacity increased by approximately 50% in 2023, reaching nearly 510 gigawatts (GW). This represents the highest growth rate in the past twenty years. The IEA forecasts that by 2028, global renewable energy capacity will expand to 7,100 GW, which is 2.5 times the current capacity. The report highlights a significant milestone: by 2025, the IEA expects renewable energy sources to surpass coal in terms of global energy production [1]

In addition to capacity growth, the cost of photovoltaic modules has dropped by about 50% compared to 2022 prices. This substantial price reduction will likely further drive the adoption of solar energy, making it an increasingly viable option for both developed and developing nations.[1]

The global energy demand is rapidly increasing, with multiple models suggesting the need for 75 TW of photovoltaic capacity by 2050. This ambitious target requires an installation rate of 1 TW per year. To achieve this, not only must we scale up installations, but also we need to improve the efficiency of photovoltaic modules. While single-junction silicon solar cells are nearing their theoretical efficiency limits, tandem solar cells, which utilize two junctions to capture a broader spectrum of sunlight, offer the potential for significantly higher efficiencies and a reduced carbon footprint. [2]

Tandem solar cells are emerging as a key technology for the future of solar energy. By enhancing efficiency, these cells can help lower the overall cost of solar power, making it more accessible and sustainable on a global scale. [2]

The advancement of tandem solar technologies represents more than just a technological improvement; it is a critical step toward achieving the necessary energy transition. By delivering higher efficiencies, tandem cells can play a pivotal role in establishing solar energy as a dominant and viable component of the global energy mix.

1.2 Solar spectrum and Air mass

The sun's emissions are quite varied, going from X-rays to radio waves, but the peak of the irradiance of solar radiation is in the visible wavelengths.[3]

The overall radiation spectrum of the Sun closely follows that of a black body with a temperature of approximately 6000°K.

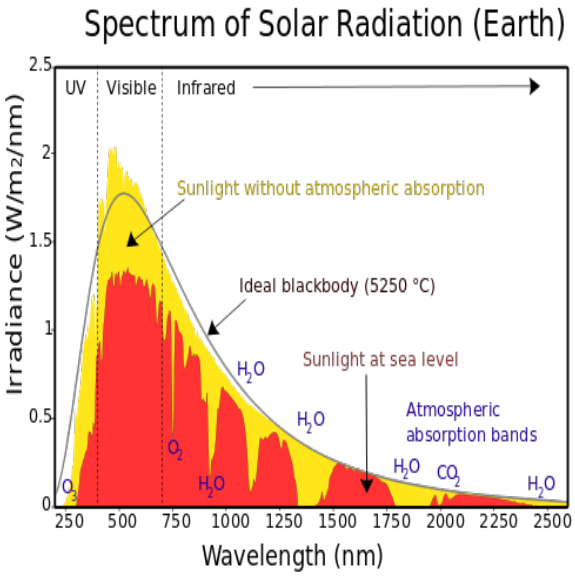

Figure 1.1: Solar spectrum, from Penn State College[3]

As showing in Fig. 1.1, not all of the Sun's emitted power reaches the Earth's surface; much of it is lost due to scattering and absorption within the Earth's atmosphere. The **air mass (AM)** represents a quantification of the power reduction of the light due to absorption caused by its passing through the atmosphere.

$$\mathrm{AM} = \frac{1}{\cos(\alpha)} \tag{1.1}$$

where α represent the angle with respect to the vertical position (zenith angle).

It can also be described as the normalized path length that the light takes through the atmosphere with respect to the shortest one possible (i.e., the sun vertically above). [4]

- **AM0**, represent the solar spectrum outside the Earth's atmosphere and is used for characterizing solar cells designed for space applications
- **AMD**, where D stands for direct, includes only direct radiation.
- **AMG**, where G stands for global, includes both diffused and direct radiation.

From the U.S. Energy Information Administration (EIA), "A photovoltaic (PV) cell, commonly called a solar cell, is a nonmechanical device that converts sunlight directly into electricity" [5]. These devices exploit the **photovoltaic effect**, shown in Figure 1.2.

The key to a solar cell is an absorbing material, specifically a semiconductor. Due to the duality of light, it can be seen both as a wave and as particles. These particles are called photons, and each of them is characterized by a different amount of energy [6]. When light impinges on a cell, it can be either reflected, transmitted, or absorbed by the semiconductor. Only the absorbed photons are able to transfer their energy to the electrons in the semiconductor material. If the energy is greater than the bandgap

energy, the electrons will be able to move from the valence band to the conduction band, creating free carriers—electrons and holes.[7].

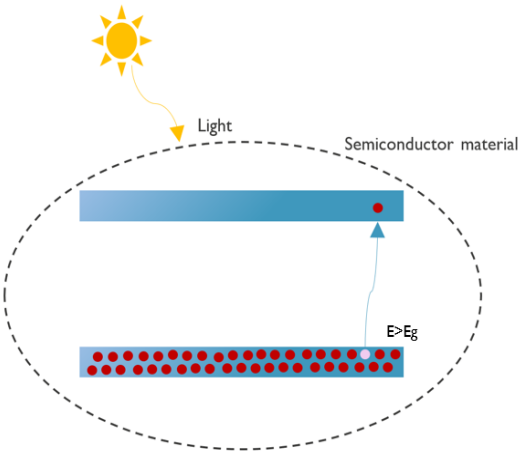

Figure 1.2: Representation of the photovoltaic effect

1.3 Basic working principles of solar cells

To ensure the power generation from a solar cell, it is crucial not only to harness photon energy to create electron-hole pairs but also to effectively extract these carriers and direct them into the external circuit.

Treating the semiconductor surface properly is essential for allowing the carriers to migrate to the cell's surface. This is achieved by incorporating transport materials: Electron Transport Material (ETM) to facilitate the extraction of electrons, and Hole Transport Material (HTM) to assist in the extraction of holes. These materials help guide the carriers towards the conductive metal contacts, where the current can be extracted, as shown in Fig. 1.3.

To separate and utilize these carriers efficiently, a typical solar cell employs both n-type and p-type semiconductors, forming a p-n junction. When light is absorbed in the cell, creating electron-hole pairs, the built-in electric field at the p-n junction drifts the electrons toward the n-type side (which has an excess of electrons) and the holes toward the p-type side (which has an excess of holes). The n-type semiconductor, due to energy level alignment, selectively transfers electrons and directs them to the external circuit. Subsequently, the p-type semiconductor, selectively transfers these electrons back into the valence band, thereby completing the circuit.

The majority of photovoltaic energy conversion systems rely on a p-n junction configuration. [8]

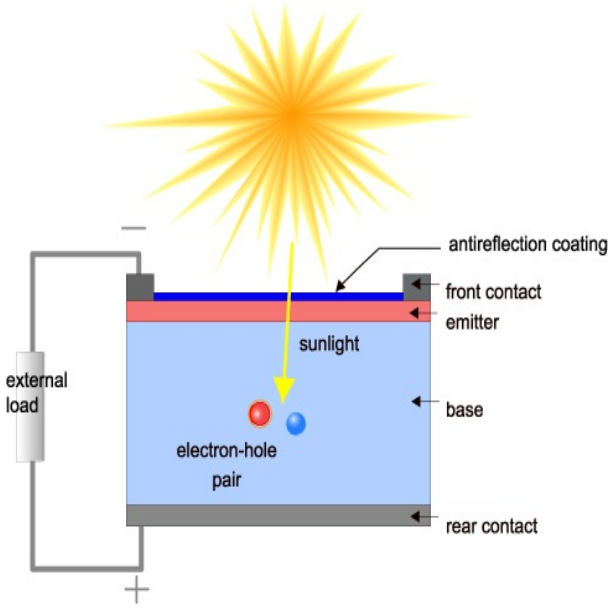

Figure 1.3: Representation of solar cell, [9]

1.4 Quantifying Solar Cell Performance:Figures of Merit

The evaluation of cell performance is crucial for research and development in the field of photovoltaic technology. This section aims to provide a comprehensive overview of the key performance indicators used to quantify solar cell performance.

In order to evaluate, sort and compare solar cells, it is essential to examine their performance characteristics under standard test conditions (STC). One of the most informative approaches for this purpose is the I-V curve, which plots the current (I) against the voltage (V) of the solar cell. By analysing the I-V curve, one can identify key performance indicators such as **short circuit current** (Isc), **open circuit voltage** (Voc) and **maximum power point** (MPP). These points on the curve are essential for assessing the efficiency and effectiveness of the solar cell, providing insight into its overall performance and suitability for different applications.

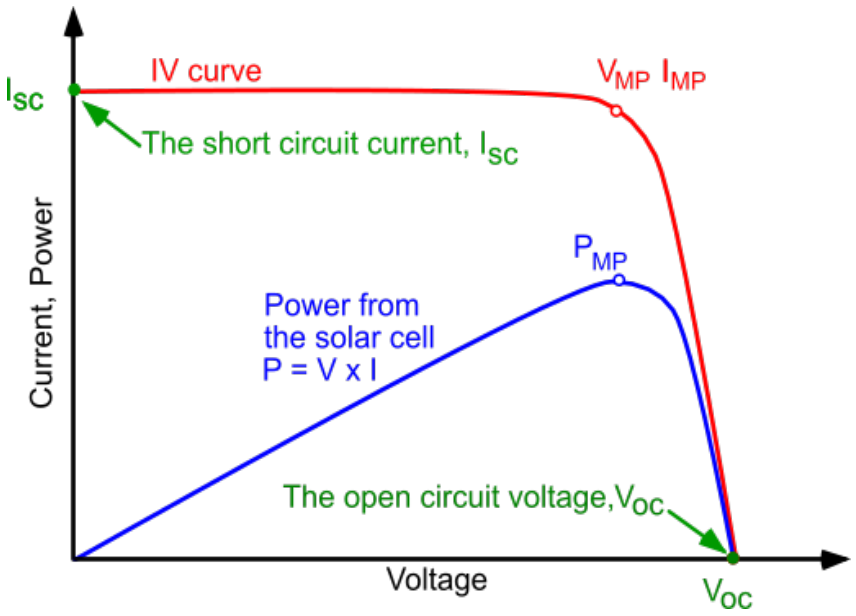

Figure 1.4: I-V and P-V curves, from PVEducation [10]

The **Open Circuit Voltage** (Voc) is the maximum voltage that develops across a solar cell when it is not connected to any load. It is a result of the forward bias created by the light-generated current at the solar cell junction.

The **Isc** is the current flowing through the cell in a short-circuit state (the voltage across the cell is 0). It is caused by the generation and collection of light-generated carriers.

Sometimes defined as Jsc or current density, which also takes into account the dimensions of the cells, allowing a comparison even between cells of different dimensions.

$$J_{sc} = \frac{I_{sc}}{\text{Area}} \quad \left(\frac{\text{A}}{\text{m}^2}\right) \tag{1.2}$$

By plotting the power curve on the P-V graph, it is possible to identify its maximum power output, called the **Maximum Power Point** of the cell. From this point, it is possible to identify the voltage at the maximum power point (Vmpp) and the current at the maximum power point (Impp).

$$P_{MPP} = I_{MPP} \cdot V_{MPP} \tag{1.3}$$

The **Fill Factor (FF)** quantifies the efficiency of the solar cell in converting the electrical power available from the solar cell into useful output power. Graphically, it represents how square the I-V curve of the solar cell is. It is visually interpreted as the area of the largest rectangle that can fit inside the curve, giving an indication of how close the cell's performance is to the ideal case where the I-V curve would form a rectangle with the maximum possible area.

Mathematically, it is defined as the ratio of the maximum power point to the product of the Voc and the Isc. The fill factor formula is:

$$FF = \frac{P_{MP}}{I_{SC} \cdot V_{OC}} = \frac{I_{MP} \cdot V_{MP}}{I_{SC} \cdot V_{OC}} \tag{1.4}$$

The **Power Conversion Efficiency (PCE)**, often referred to just as efficiency, represents the ratio between the output power of the solar cell and the input power (the sun power reaching the cell).

$$\text{PCE} = \frac{P_{out}}{P_{in}} \times 100\% \tag{1.5}$$

where P_{out} is the electrical power output of the solar cell, and P_{in} is the incident solar power.

Quantum efficiency

The **Quantum Efficiency** (QE), is an important figure of merit for solar cells. It quantifies the ability of a solar cell to convert incident photons into charge carriers (electrons or holes), that will then contribute to the electric current. It is defined as the ratio of the number of charge carriers collected by the solar cell to the number of incident photons for a given energy, and it is plotted as a function of either wavelength or energy.

The ideal QE curve is quadratic. This is because QE is zero for photons with energy less than the bandgap energy, and ideally it should be one for photons with energy equal to or higher than the bandgap energy.

In reality, the QE curve is never perfectly quadratic due to non-idealities such as recombination effects. These non-idealities reduce the collection efficiency of the carriers generated by the photons. QE can be thought of as the probability of collecting carriers generated by photons of a given wavelength, integrated over the thickness of the device and normalised to the number of incident photons of that wavelength. [11]

The **External quantum efficiency** (EQE) is defined as the ratio of electrons collected per incident photon under short-circuit conditions.[11]

$$\text{EQE}(\lambda) = \frac{\text{collected electrons}}{\text{incident photons}}\Big|_{\text{shortcircuit}} \tag{1.6}$$

The **Internal quantum efficiency** (IQE) quantifies the collectable carriers generated by photons absorbed by the solar cell, excluding those that are reflected or transmitted. It is defined as the ratio of collected electrons to absorbed photons.[11]

$$\text{IQE}(\lambda) = \frac{\text{EQE}(\lambda)}{1 - R(\lambda) - T(\lambda)} \tag{1.7}$$

1.5 Silicon solar cells

Monocrystalline solar cells dominate the market due to their high efficiency at low cost and mature manufacturing process.

To obtain a basic silicon solar cell, the starting point is a silicon wafer of sufficient purity, and then undergo a doping process to create a p-n junction, first a p-type doping, then an n-type doping. The p-type doping is obtained by introducing atoms of group III elements; with respect to Si, they have one valence electron less, which allows a positive charge behaviour; the elements most commonly used are boron and gallium. The n-type is obtained by introducing elements of group V, because they have one valence electron more than Si, providing an extra electron and giving a negative charge behaviour. The most commonly used elements are phosphorus and arsenium. At the moment the highest efficiency reached for silicon solar cells is 27.1 % and it was achieved by LONGI Solar (also shown in FIG. 2.1).

1.5.1 Shockley-Queisser limit

In 1960, Shockley and Queisser published a paper in which they searched for a theoretical upper limit to the efficiency of solar cells, assuming that the only recombination effect was the radiative one. They concluded that this upper limit is highly depending on the energy bandgap of the semiconductor. The maximum efficiency achievable for a p-n junction solar cell with an energy bandgap of 1.1 eV, like Silicon, is equal to ~ 30%. [12] Today, the goal is to overcome this limit. Researchers are using a variety of approaches, among which the most popular options are the use of novel materials and multi-junction solar cells.

1.6 Multi-junction solar cells

A solution to overcome the Shockley-Queisser limit is multi-junction solar cells (also known as **tandem**, when double junctions are applied), which maximize the efficiency of solar energy conversion by capturing photons with a wider range of wavelengths. Although this field is still at an early stage of development, there is significant potential for improvement. Multijunction solar cells are a series of multiple sub cells, each is capable of absorbing a different wavelength in the solar spectrum, allowing the Shockley-Queisser limit to be overcome. The wide bandgap cell can absorb the higher energy photons, so it is positioned as the first cell that the incident light encounters. If the energy is lower than the bandgap of this cell, it is transferred to the cell below, which has a lower bandgap and is able to absorb photons with longer wavelengths, and so on until the last cell in the stack. [13]

1.7 Thin film solar cells and emerging materials

In an **indirect** bandgap material, such as silicon, the minimum energy level of the conduction band and the maximum energy level of the valence band are not at the same value of electron momentum. In an **indirect bandgap** material, as shown in Fig. 1.5b, the transition of an electron from the valence band to the conduction band requires not only the absorption of a photon to provide the necessary energy, but also the involvement of a phonon to conserve momentum. This additional requirement makes the generation of electron-hole pairs slower and less likely in indirect semiconductors. A **direct bandgap** material, as shown in Fig. 1.5a, does not require the assistance of a phonon to create an electron-hole pair, leading to more efficient light absorption and high energy conversion efficiency. Consequently, in optoelectronic devices, the distinction between an indirect and a direct bandgap semiconductor is crucial.[14] Given the better optoelectronic properties of direct bandgap materials, it is possible to use absorber materials much thinner than silicon.

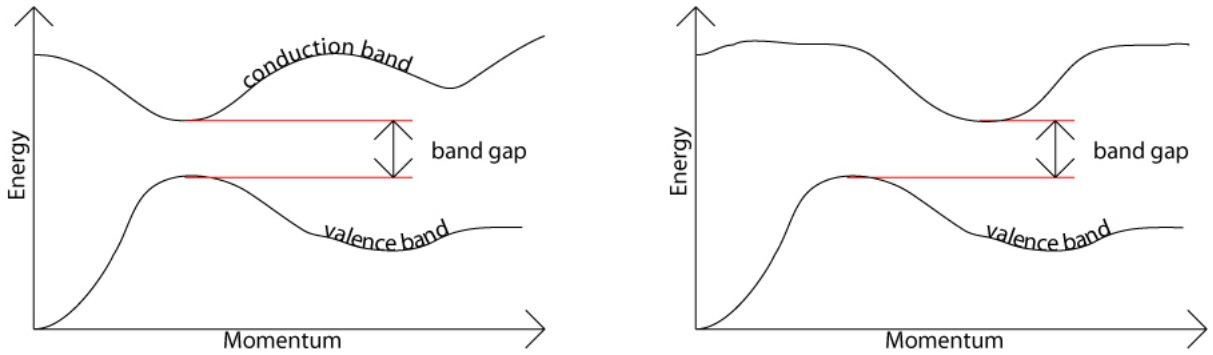

(a) Direct bandgap (b) Indirect bandgap

Figure 1.5: Representation of the Bandap, [14]

The III-V semiconductors, in particular gallium arsenide (GaAs), are characterised by a **direct** bandgap. These materials have emerged as promising candidates for high-efficiency solar cells and optical devices in general. Despite their superior performance, the high cost of these materials currently limits their widespread use in specialized applications such as space technology.

While crystalline silicon solar cells continue to dominate the market, the share of thin-film solar cells is growing gradually, driven by intensive research and development efforts.

This innovative approach to solar cell manufacture uses a few micron to submicron-thin photon-absorbing materials, as opposed to the thick layers of silicon traditionally used. These thin films can be deposited on flexible substrates, opening up new possibilities for lightweight, versatile solar technologies. This approach offers several advantages, including reduced material usage, lightweight design, and potential cost reductions. [15] Common materials used in thin-film technology include cadmium telluride (CdTe), copper indium gallium selenide (CIGS), and **halide perovskites**.

Chapter 2

Perovskite-based single and multi-junction solar cells

This chapter focuses on perovskite-based solar cells, both single-junction and multi-junction, examining their chemical structures, fabrication methods, and characterization techniques.

Perovskites are materials that have attracted attention in the optoelectronic and photovoltaic fields due to their unique physical properties, including high absorption coefficients over a range of wavelengths, which is crucial for solar cell applications, high dielectric constants, ferroelectric properties and low processing costs. These properties are very attractive for solar cell apllications.

The figure 2.1 illustrates the development of both perovskite-based solar cells and silicon cells. Over the past decade, there has been a substantial increase in efficiency. For instance, the record efficiency for perovskite cells rose from 14.1 % in 2013, achieved by EPFL, to 26.7 % in August 2024, set by USTC.

In the silicon-perovskite tandem field, the current highest efficiency is held by Longi, a 33.9 % record cell.

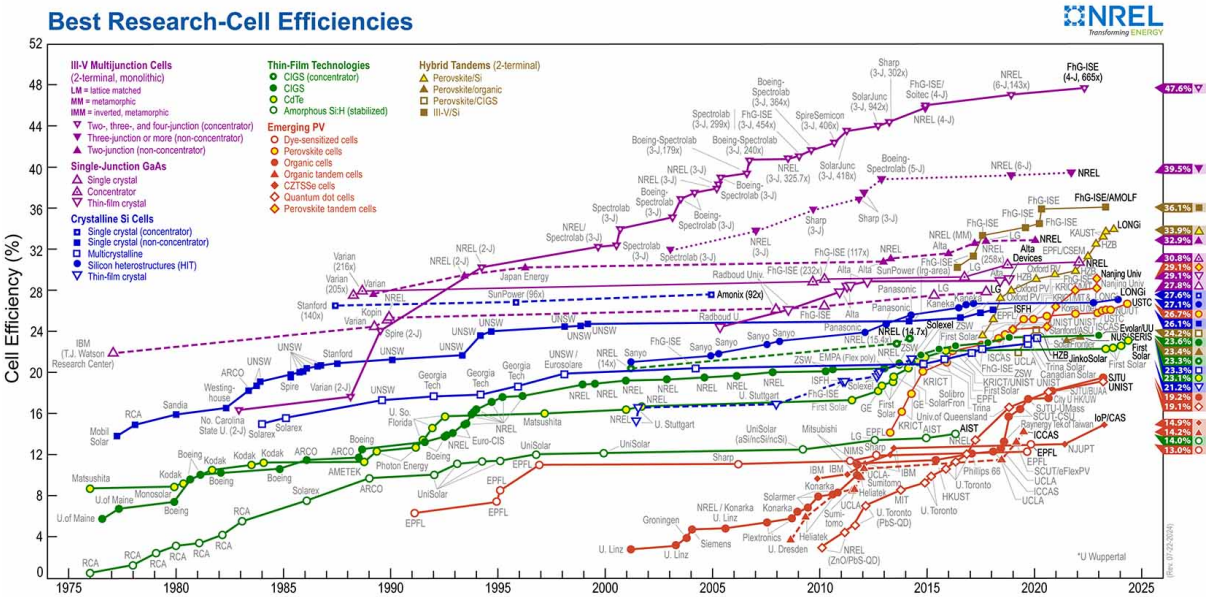

Figure 2.1: Best Research-Cell Efficiency Chart, from NREL [16]

2.1 Perovskite chemical structure

The crystal structure of a perovskite consists of a network of corner-sharing BX_6 octahedra, which typically crystallise with a general ABX_3 (or equivalent) stoichiometry. Deviations from this ideal stoichiometry can occur when the A and B cation sites become partially or completely vacant, leading to the formation of vacancy-ordered perovskites. Additionally, stoichiometric variations can occur by substitution of the A or B cations with a combination of other cations, which may have different valences but maintain overall charge neutrality. [17]

The most symmetrical structure is known as "aristotype" perovskite, but due to distortions in the crystal (i.e. lattice distortions, vacancies, etc.) most perovskite structures have reduced symmetry. [17] The photoactive layer in perovskite solar cells (PSCs) is usually made of a metal halide perovskite (MHPs) with the general formula ABX_3, where:

- **A** represents the larger cation, which can be either a monovalent organic or inorganic ion. The most common organic cations are methylammonium ($CH_3NH_3^+$) and formamidinium ($CH(NH_2)_2^+$), while the most common inorganic cation is cesium (Cs^+);
- **B** represents the smaller cation, usually lead (Pb^{2+}) or tin (Sn^{2+}), which are divalent metals;
- **X** is the anion, usually oxide or halogen, more often a halide such as iodide (I^-), chloride (Cl^-) or bromide (Br^-);

Chemical composition engineering allows tuning of the perovskite band gap, which is typically around 1.5-1.6 eV. Perovskites with a wide band gap (WBG) of 1.65-2 eV, which have a high bromine (Br) content, are often used as top cells in tandem configurations. These WBG perovskites are generally characterised by a cubic crystal structure. [18]

Perovskites can be broadly classified into chalcogenide perovskites (AMO_3) and metal halide perovskites (ABX_3), with different properties and applications in photovoltaic and optoelectronic devices.

[19] [20]

2.2 Perovskite Absorber Layer

As part of thin-film PV technologies, perovskite solar cells have attracted great attention because of their many advantages. One of the key strengths of PSCs is their high theoretical efficiency, makes them a strong candidate for next-generation solar cells.[18]

Metal Halide Perovskite, due to their direct bandgap are characterized by a higher absorption coefficient than most semiconductor (including silicon). This property makes perovskites highly efficient light absorbers, allowing for the deposition of a thinner photoactive layer (typically 300–600 nm) in the PSCs with respect to other photovoltaic technologies such as silicon wafers, which require thicknesses ranging from 150 to 300 μm.

However, despite these promising features, the technology is not yet mature. There are several challenges, mainly related to scalability and stability issues.

2.2.1 Perovskite-Silicon tandem solar cells

A perovskite-silicon tandem solar cell is a multi-junction cell that combines two types of solar cell: a crystalline silicon solar cell and a perovskite solar cell. The configuration is as follows:

- **Bottom cell**: Silicon solar cell, since they are more efficient at absorbing lower-energy photons from the solar spectrum.
- **Top cell**: Perovskite solar cell, they can be optimized to absorbed higher energy photons, depending on the desired bandgap

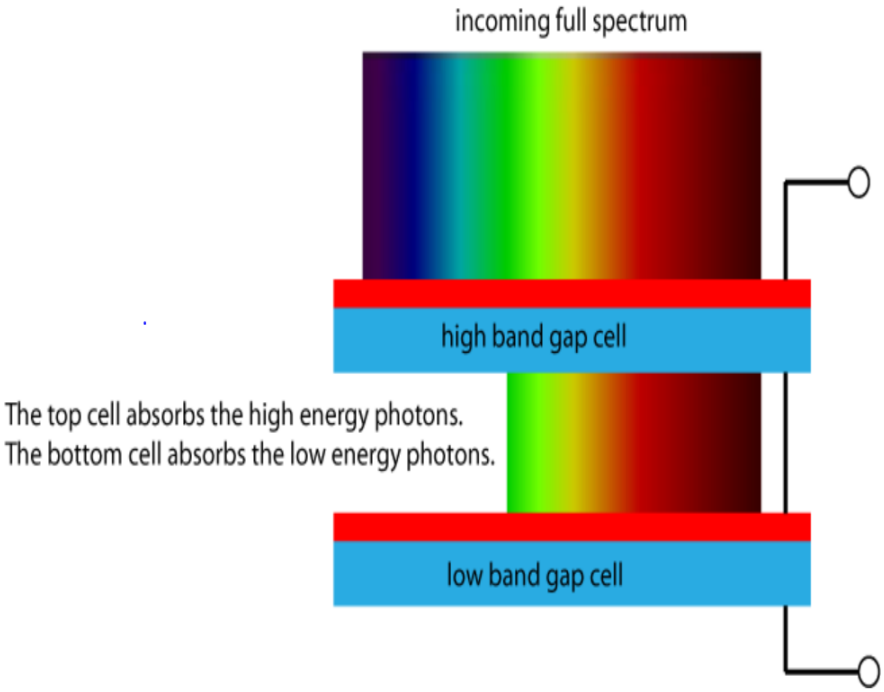

Figure 2.2: Representation of tandem solar cells, from PVEducation [21]

This configuration allows for higher efficiency because it utilises the complementary absorption spectra of both cells.

One step method

In the one-step process, the perovskite is realised by direct deposition of a precursor solution. This can be achieved using several techniques, including blade coating, spray coating, and spin coating. For large area scalable deposition, blade coating and slot die coating are the main techniques of choice, usually coupled with gas or vacuum assisted quenching. The thickness of the film is determined by the concentration of the precursor, the speed of the blade (or slot die), and the gap between the substrate and the blade (or slot die). [18] Usually post-deposition annealing is required.

Two-Step Deposition

In the two-step process, the lead halide layer is deposited by solution process (e.g. spin coating, blade coating, slot die coating) or vacuum deposition, and then the organic cation

solution is deposited by either olution or vacuum processing. To enhance the quality of the perovskite films produced, various techniques can be employed. These include adding precursor additives, performing solvent annealing, and making surface modifications. It is important to note that these techniques are not limited to the two-step process; they can also be applied to one-step or other deposition methods to improve the performance and quality of perovskite layers.

In this work the two-step deposition approach was used. In the following sections the fabrication steps of the perovskite solar cells structure will be introduced.

2.3 Fabrication of perovskite single-junction cells

Silicon bottom cells, due to their fragility and higher cost, are more delicate and expensive than glass substrates. Despite the ultimate goal is to produce tandem solar cells, for research purposes it is preferable to work on glass first to develop perovskite solar cells and then move on to silicon.

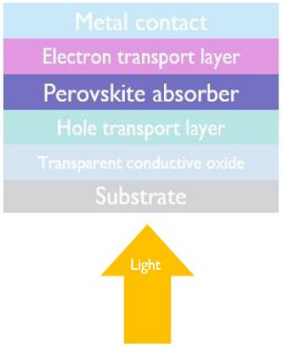

Figure 2.3: A schematic diagram of inverted p-i-n perovskite solar cell.

In Fig. 2.3, it is possible to see a generic PSC structure. The single-junction solar cells fabricated for this study are based on 3x3 cm glass substrates with patterned ITO. For each substrate, 12 cells with an active area of 0.125 cm^2 are produced.

The first step in the fabrication of perovskite solar cells is a meticulous cleaning process. The substrate is first scrubbed with water and soap, then immersed in a soap solution and placed in an ultrasonic bath. Then sonication with each of these solvents is carried out for 10 minutes: deionized water, isopropanol and acetone.

Once the substrate is cleaned and dried, the next step involves depositing the **charge transport layer**.

The **charge transport layers**, can be divided into hole transport layer (HTL) and electron transport layer (ETL). These layers facilitate the flow of holes (or electrons) to the electrical contacts while preventing the flow of opposite charges, thereby improving the interfaces between the photoactive material and the electrodes, reducing recombination losses.

2.3.1 Hole Transport Layer

In the p-i-n configuration (shown in Fig. 2.3), the HTL plays a key role as it is the first layer on top of the transparent conductive oxide (TCO). In our study, the TCO chosen

is indium tin oxide, ITO. The HTL is not only the first layer, but also the substrate on which the perovskite layer is deposited, which requires a suitable material as this layer will influence the morphology of the perovskite layer itself. Its role is not limited to hole collection and blocking electrons, but also to improving the quality of the interface by reducing defect states. [18]

Various HTLs are currently used, including both organic and inorganic materials. A class of inorganic HTL are the **metal oxides**. They make good HTL because of their chemical stability, good transmittance, scalability and low cost. However, they present specific challenges, mainly due to surface defects.

The most promising class of inorganic HTL for p-i-n PSC is represented by NiOx (and its variant, but in this study NiOx was used) due to its suitable work function, high optical transmittance and intrinsic chemical, thermal and light stability. [18]

In this work, the NiOx layer is deposited onto the substrates by direct current (DC) reactive sputtering of a Ni target in pure oxygen plasma. To tune the optoelectronic properties of this layer, an additional annealing step (300 ° C for 20 min in air) is required. The annealing step improves crystallinity, tune the optoelectronic properties and reduces Ni^{3+} defects. Eventually, the annealing step could be avoided through the use of RF sputtering of NiOx target for NiOx.

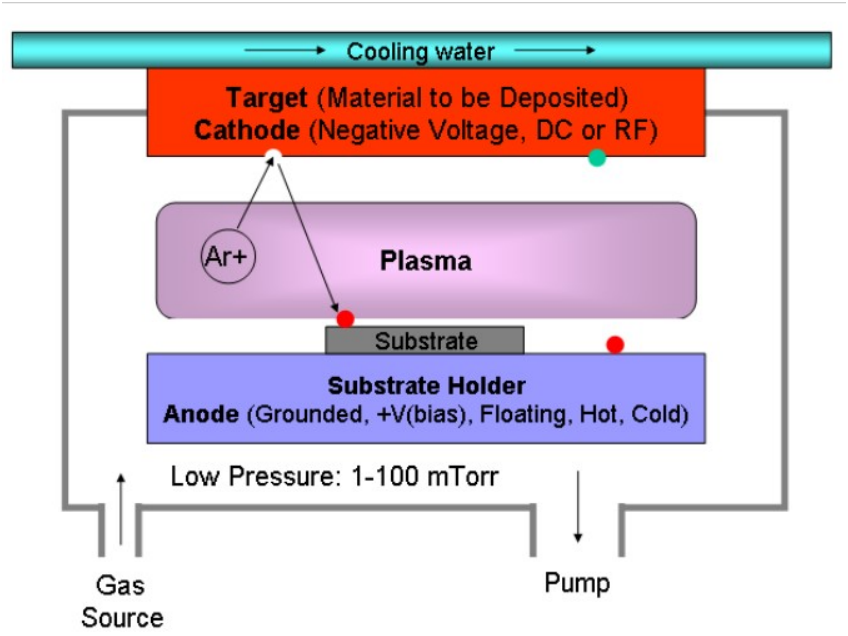

Figure 2.4: A schematic diagram of DC sputtering chamber and process [22]

Sputtering (shown in Fig. 2.4) is a physical vapor deposition (PVD) process that involves bombarding the target material with high energy particles to eject atoms from its surface, which are then deposited onto the substrate. This ion bombardment is achieved typically using an Ar^+ plasma, an inert gas that will not react with the target and/or the substrate. While sputtering provides excellent adhesion of the deposited film, it can also potentially damage the substrate. [22]

Self-assembled Monolayers

As organic HTM, self-assembled monolayers (SAMs) are among the most popular choices. SAMs are single layer (i.e. monolayer) molecules capable of self-assembly, the

process of forming an organised structure (or pattern) from a disordered system of components without the need for external guidance.[23] This is done by either liquid or vapour phase deposition onto the surface of the substrate.[24]

The self-assembly process can be divided into three phases: adsorption, self-assembly and formation of the final monolayer structure. SAM molecules are composed of three main components:

- **Anchoring**: promotes the attachment of the SAM to the substrate.
- **Spacer**: The length of the chain can vary, helping to stabilise the monolayer.
- **Terminal Function**: This terminal can be modified to give specific surface properties.

SAMs are highly effective as HTLs due to their unique properties: they have the ability to transfer holes and prevent charge accumulation at the interface, they can be deposited in ultrathin layers that allow negligible parasitic absorption, and they are chemically stable under perovskite precursor deposition, making them an ideal HTL for PSC. SAMs also do not require additional doping and are compatible with a wide range of substrates. They can be deposited using a variety of deposition techniques and can be dissolved in 'green solvents' such as isopropanol or, in the case of this study, ethanol.

Currently, SAMs are widely used for both single and tandem PSCs. [18] Interest in the use of SAMs peaked when it was reported that a family of carbazole-based molecules with a phosphonic acid group (namely, 2PACz, MeO-2PACz and Me-4PACz, shown Figure 2.5) have groups that absorb onto the surface of the substrate. [18]

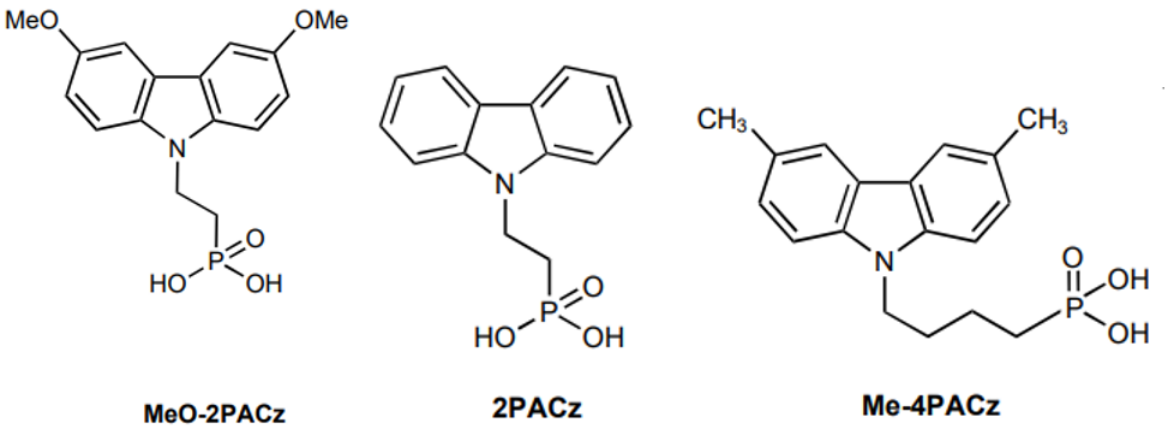

Figure 2.5: SAM molecules, [18]

In this study, we specifically used Me-4PACz. It was deposited using two methods: spin-coating and thermal evaporation. For spin-coating, the process involved an initial dynamic spin-coating of the SAM followed by a dual spin-coating step with ethanol—both static and dynamic—to wash the surface and remove excess Me-4PACz molecules. On the other hand, when thermal evaporation was employed, the washing step was not necessary.

Spin-coating is a technique used to deposit layers with thickness in the nanometre to micrometre range. A liquid solution is dropped to the sample, which is then spun at

very high speeds. The centrifugal force generated by the spin coater ensures that the coating is uniform and thin. Furthemore, the thickness can be adjusted by varying the parameters of the spincoater and/or the solution being spincoated.

Figure 2.6: A schematic illustration of spin coating process.

- The dynamic spincoating consists of dropping the solution onto the substrate while it's spinning.
- The static spincoating process involves a two-step approach: first, the solution is dropped on the substrate, and then spinning phase is started.

The deposition is usually followed by a waiting period or thermal annealing to ensure complete evaporation of the solvents used.

Thermal evaporation is a process conducted under low pressure conditions (∼5x10-5 Pa) in which vapour is produced by heating a solid material source. To achieve this, a crucible containing the source is used. The vapour particles are deposited on the substrate, transforming from a vapor to a solid state. [22]

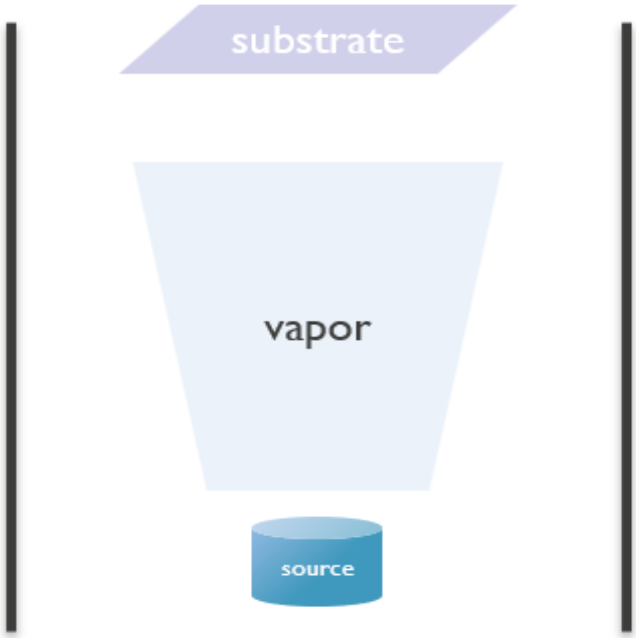

Figure 2.7: Thermal evaporation representation

The low pressure working condition is necessary to facilitate the movement of the particles to reach the substrate.

To ensure the correct evaporation conditions, a Quartz Crystal Micro-balance (QCM) is used to control the process parameters, i.e. evaporation rate and thickness. [25]

2.3.2 Perovskite absorber layer

To maximize the benefits of the tandem configuration it is necessary to use the appropriate depositions technique, since it influences the characteristics of the cells. An optimal deposition technique enables scalability and reproducibility to be achieved at low cost. The right process is essential to obtain the desired physical characteristics, such as large grain size, reduced grain boundaries, and fewer defects. Deposition techniques can be divided into two main categories: one-step and two-step. In this work, the method chosen to produce the perovskite layer is the **hybrid method**, which combines two distinct processes: a high-vacuum thermal co-evaporation of the inorganic precursors followed the spin-coating of the organic precursors.

In the **co-evaporation step**, the inorganic precursors lead iodide (PbI_2) and cesium bromide (CsBr) are simultaneously thermally evaporated. The substrates are kept at a low temperature (-5 ° C) during deposition.

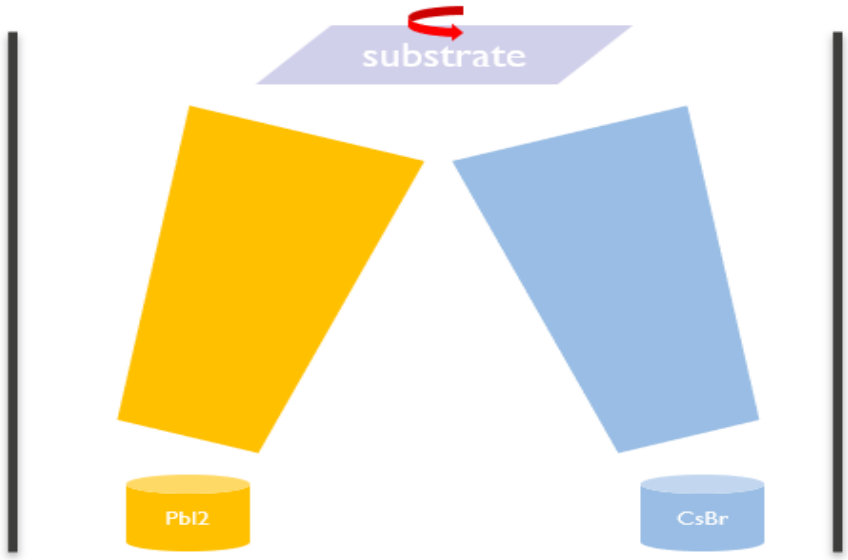

Figure 2.8: Co-evaporation setup

After co-evaporation, the next step is the **spin-coating** of the solution containing the organics,specifically formamidinium iodide (FAI), formamidinium bromide (FABr), and methylammonium chloride (MACl). The solution was prepared by carefully weighing the powders and dissolving them in ethanol, aiming for a final perovskite with a bandgap of 1.67 eV.

To ensure the correct deposition of the organics and the correct evaporation of the solvent,following spin-coating, there is a 10-minute waiting period before the substrate undergoes annealing at 130 °C for 20 minutes.

The hybrid method has gained significant interest recently due to its numerous advantages. It provides precise control over the growth environment and the deposition rate of various inorganic perovskite precursors, ensuring highly reproducible film thickness and uniformity across large areas. Additionally, it guarantees complete and conformal coverage of the substrate with surface roughness. This technique also supports the use of non-hazardous solvents and straightforward upscaling. [26]

2.3.3 Electron transport layer

Electron transport layer (ETL) materials used for p-i-n PSCs are mainly fullerene-based n-type conjugated polymers and n-type metal oxides. They need to have different characteristics, such as suitable energy level, high electrical conductivity and mobility, and easy fabrication.

Popular ETL materials are fullerene-based, including C_{60}, C_{70}, due to their high electron mobility and low temperature processing. However, their cost remains a significant drawback. The fullerene layer is usually followed by a buffer layer that ensures energy alignment with the counter electrode, such as bathocuproine (BCP), used in this study. Other inorganic alternatives are often used, such as SnO_2, ZnO, and TiO_x, which could be used to replace the BCP layer. [18] In this study, C60 was selected as the electron transport layer. To enhance the interface with the perovskite layer, a lithium fluoride (LiF) buffer layer was applied between the perovskite and C60. Similarly, a BCP buffer

layer was used to improve the interface between C60 and the metal contacts. Both buffer layers were deposited via thermal evaporation.

Figure 2.9: ETL stack

2.3.4 Metal contacts

The metal contacts are created through the thermal evaporation of silver under high vacuum conditions. Masks are employed to define the contact areas precisely.

Figure 2.10: Opaque cell stack

In Fig. 2.11 it is possible to see the completed cell.

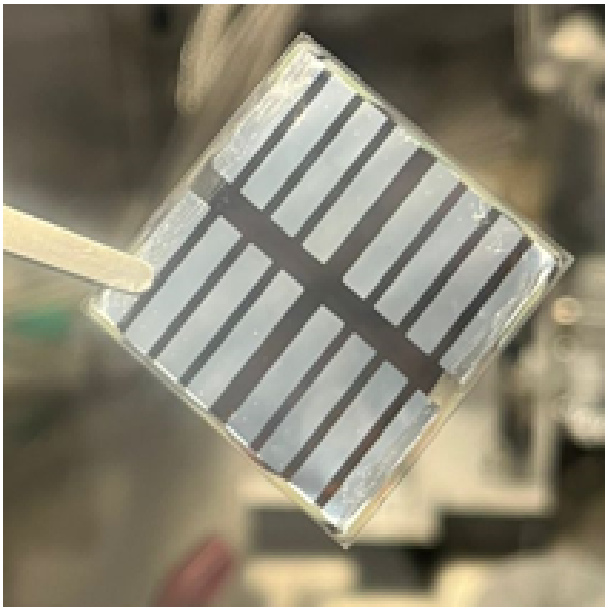

Figure 2.11: A photograph showing the rear electrode side of a single-junction perovskite solar cell fabricated in this work.

2.3.5 Semitransparent single-junction solar cell

In Fig. 2.12, the layer stack of a semitransparent single-junction solar cell is depicted. In this configuration, an additional indium tin oxide (ITO) layer is deposited between the electron transport layer (ETL) and the metal contacts using sputtering

Figure 2.12: Semitransparent perovskite cell stack design.

2.4 Fabrication of tandem cells

In perovskite-silicon solar cells, the perovskite solar cells are fabricated using a silicon solar cell as the substrate instead of glass. As shown in Fig. 2.13, the fabrication steps of the perovskite top cell are similar to those used for creating a single-junction PSCs. The

process begins with a standard silicon solar cell, on which ITO is deposited on the back side through sputtering, followed by the deposition of silver to form the back contacts. On the top side, ITO is again deposited through sputtering,followed by the deposition of the HTL, Me-4PACz in this case. The perovskite layer is then deposited using the hybrid method: first, the inorganic precursors are thermally evaporated, and then the organic solution is spin-coated on top. This is followed by the deposition of the ETL, and finally the metal contacts are added to realize the front contacts. An antireflection coating (ARC) is also used in the structure as depicted in Fig. 2.13. [27]

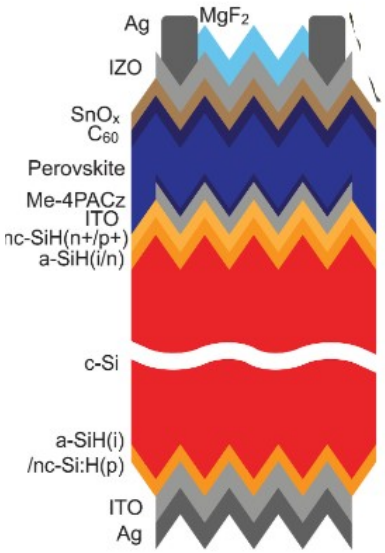

Figure 2.13: Silicon/perovskite tandem solar cell [27]

2.5 Characterization

A fundamental step in research is the comprehensive study of the fabricated cells to gain a deeper understanding of their performance. Characterization is a crucial to gain understanding on the optical behavior, as well as the electrical and physical properties of the materials and solar cells.

Through appropriate characterization techniques, we can evaluate the figure of merit such as efficiency, fill factor, open-circuit voltage, and short-circuit current. These metrics are essential for evaluating the overall performance of the fabricated solar cells and their effectiveness in converting solar energy into electrical energy.

2.5.1 Solar Simulator

A solar simulator, as the name suggests, is a characterisation device that emulates the light emitted by the sun. It can be used in several ways and in several areas, but in the course of this study it was used to extract the current-voltage (I-V) curve of the cells and the parameters associated with it.

To be able to confront the result, it is necessary to perform the characterisation according to the Standard Test Conditions (STC).

- **Cell temperature** equal to 25°C.

- **Solar spectrum equal** to AM1.5 for terrestrial solar cells and AM0 for the space solar cells.
- **Light intensity** equal to one sun illumination (100 mW on cm2). It is an important parameter since the solar cell efficiency depends both on the spectrum and the intensity of the incident light.

During operation, a range of voltages is applied to polarise the cells. Different voltages are applied to the junctions and the current flowing through them is then measured and the I-V characteristics recorded.

Many of them have additional features; the one used in this study also allowed temperature control through a temperature controller. Masks can also be used to change the illuminated area.

Solar simulators also vary based on the type of lamp used. In this study, a xenon lamp was employed due to its ability to provide a broad and stable spectrum that closely mimics natural sunlight.

The **Hysteresis measurements** allow for the detection of the hysteresis present in the cells.

Solar cells that preset hysteresis present a dependence of the JV curve upon the direction of the voltage sweep. Hysteresis can be caused by defects, interface properties, and charge trapping within the cells.

A maximum power point tracker (MPPT) is employed to identify the point at which the solar cell produces its maximum power. The cell is polarized following an algorithm to find this optimal point and maintain a stable power output for a specified duration, ensuring the cell operates efficiently.

Since realizing a device able to respect all this condition is quite expensive, many laboratories have "in-house" realized setup, and many times during the measurements some STC requirements are not met, so cells are often measured also by a third party, either before the purchase or to certify an actual record cell. [28] [29]

2.5.2 SEM

The scanning electron microscope (SEM) is a powerful imaging technique employed across various scientific fields to acquire high-resolution microstructure images of the samples. Unlike optical microscopes, which use visible light to view samples, SEM utilizes a beam of high-energy electron to achieve much higher resolution.[30]

The interaction between the elecontron beam and the sample generates signals that reveal information about the morphology of the sample. [31]

In this study, SEM was primarily used to analyze the morphology of the cross-sections of a co-evaporated thin PbI_2:CsBr film.

2.5.3 Photoluminescence

Photoluminescence (PL) spectroscopy is a contactless, nondestructive method for analyzing the electronic structure of materials. It is widely employed in the characterization of semiconductor materials, making it particularly suitable for analyzing the perovskite layer in solar cells.

When light impinges on a sample, it is absorbed, and the excess energy is transferred to the material in a process known as photoexcitation.

Due to photoexcitation the electrons within the material are promoted to higher energy levels, or excited states. As they return to their equilibrium states, the excess energy is released either through the emission of light (radiative processes) or without light emission (non-radiative processes). The wavelength of the emitted light can be directly related to the material's bandgap energy, providing valuable information about its electronic properties. [32]

PL spectroscopy be used in a variety of situations to have different information. In this study, **steady state photoluminescence (SSPL)** and **transient photoluminescence (TRPL)** were used to evaluate the bandgap of the fabricated perovskites.

TRPL was used to evaluate the kinetics of charge transfer and recombination, giving us the opportunity to evaluate the Shockley-Read-Hall recombination rate and the Auger recombination.

Chapter 3

Wide bandgap perovskite solar cell development by vapor-solution hybrid approach

To achieve high-performance silicon/perovskite tandem solar cells, optimization of both the perovskite material and the silicon substrate is required. Therefore, this chapter presents an examination of both the perovskite and the silicon cells, with focus on optimization of wide bandgap perovskites such as material properties and fabrication processes.

3.1 Silicon Heterojunctions Cells – Effect of Annealing Temperature

In the silicon/perovskite tandem solar cell stack, in addition to self-assembled monolayers (SAMs), NiOx is also used as the hole transport layer (HTL). NiOx requires an annealing step at 300 °C to enhance its optoelectronic properties. However, since the silicon heterojunction cell contains amorphous silicon layers that can be sensitive to high temperatures, the goal of this experiment is to assess the effects that such high temperatures might have on these layers.

The silicon heterojunction cells used in this experiment were initially fabricated at IMEC without metallic contacts. For this study, ITO was deposited on the top of the cells, followed by annealing at either 260 °C or 300 °C for 20 minutes. Subsequently, silver was deposited to form the electrical contacts.

To characterise the cells, JV measurements under 1-sun illumination were performed. The cells annealed at 260 °C, as shown in Fig. 3.1, showed better performance in terms of FF, PCE and Voc, proving that 300 °C caused too much damage to the cells.

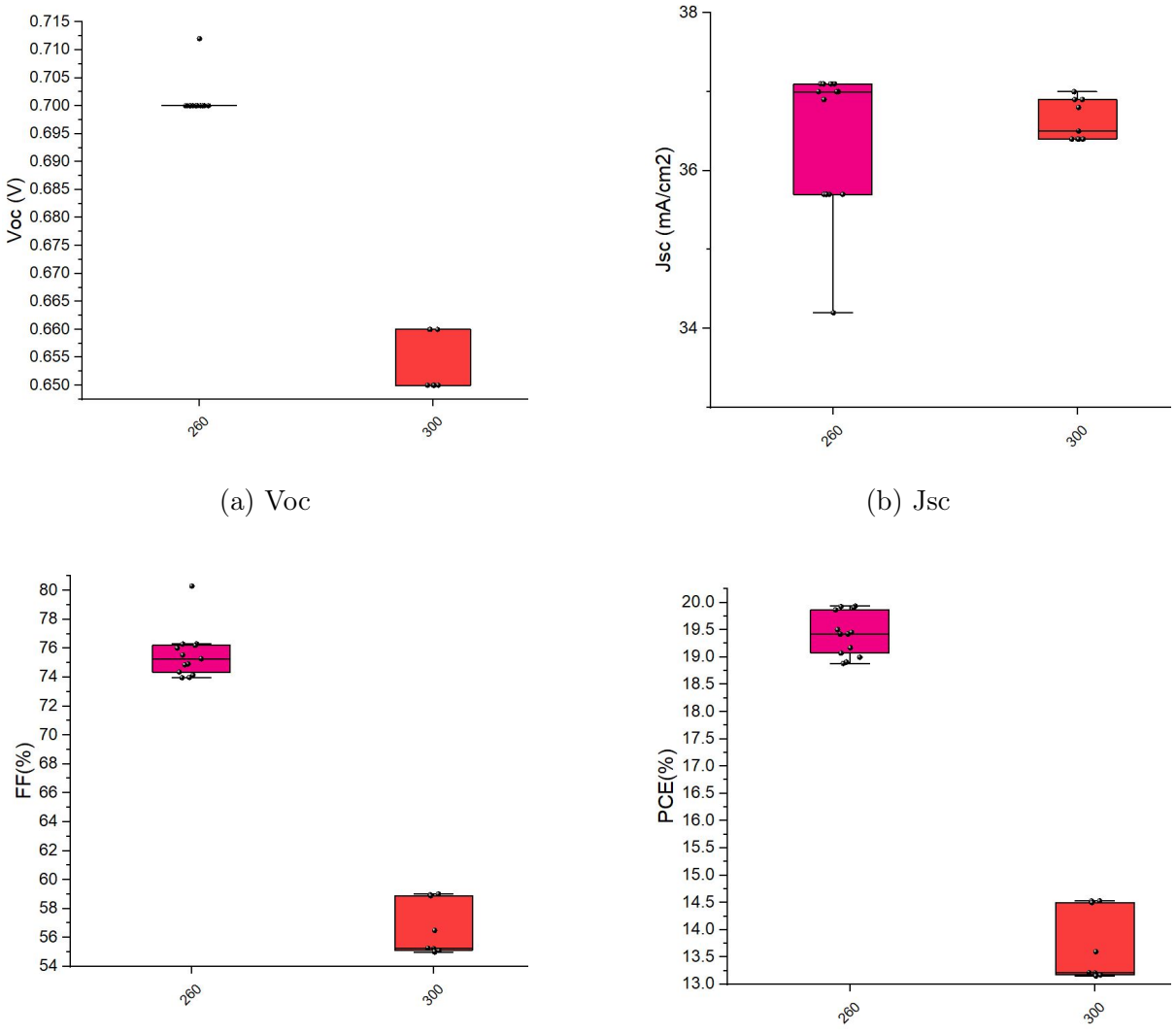

(a) Voc

(b) Jsc

(c) Fill factor

(d) Efficiency

Figure 3.1: Comparison on photovoltaic characters between silicon heterojunction cells annealed at 260 vs 300 °C.

3.2 Reflection in Silicon Solar Cells

A major source of energy loss in silicon solar cells, and in solar cells in general, is the reflection losses of incident light from the cell surface.

Several techniques have been developed to minimise reflection and increase the amount of light absorbed by the cell. The most common methods include applying an anti-reflective coating (ARC) or creating surface textures, such as geometric patterns, to trap light. In many cases, these techniques are combined to maximise efficiency.

One effective approach to reduce reflection is to etch three-dimensional pyramids onto the silicon surface, a solution of NaOH (or KOH) is used to create a surface orientation of (111). This textured surface traps more light by causing multiple internal reflections, significantly reducing reflection losses and increasing overall light absorption.

For silicon/perovskite tandem solar cells, the silicon solar cell surface on which the perovskite solar cells is deposited could be planar or textured. To lower the reflection losses,

a textured surface could be an effective way to achieve higher performance. However, the growth of a high-quality perovskite thin film on pyramids larger than the perovskite film thickness is a challenge.

3.3 Morphology study

The hybrid evaporation-spin coating method offers the possibility of depositing perovskite films conformally on textured surfaces. The aim of this study was to evaluate the deposition of PbI_2 and CsBr on textured silicon (Figure 3.2) by varying the evaporation parameters and the previously deposited layer. The morphology of the co-evaporated layer is important, as it will define the level of interaction of the organic precursors spin coated with the inorganic precursors in the evaporated film. In general, a uniform but porous layer would facilitate the infiltration of the spin coated solution and lead to a complete conversion into a perovskite phase.

Figure 3.2: A schematic diagram of silicon substrate with textured surface

Three main configurations have been analysed. The schematics of these figures can be seen in Figure 3.3:

- 3.3a, Textured silicon, sputtered ITO, sputtered NiOx, followed by co-evaporation of PbI_2 and CsBr.
- 3.3b, Textured silicon, sputtered ITO, thermally evaporated Me-4PACz, followed by co-evaporation of PbI_2 and CsBr.
- 3.3c, Textured silicon, sputtered ITO, sputtered NiOx, thermally evaporated Me-4PACz, followed by co-evaporation of PbI_2 and CsBr.

(a) (b) (c)

Figure 3.3: Schematics of the analysed configurations

The configurations were analysed by varying the co-deposition rates. The initial step involved examining the reference evaporation conditions, which consisted of a deposition rate of 1:0.3 Å/s PbI_2:CsBr and a substrate temperature of -5 °C.

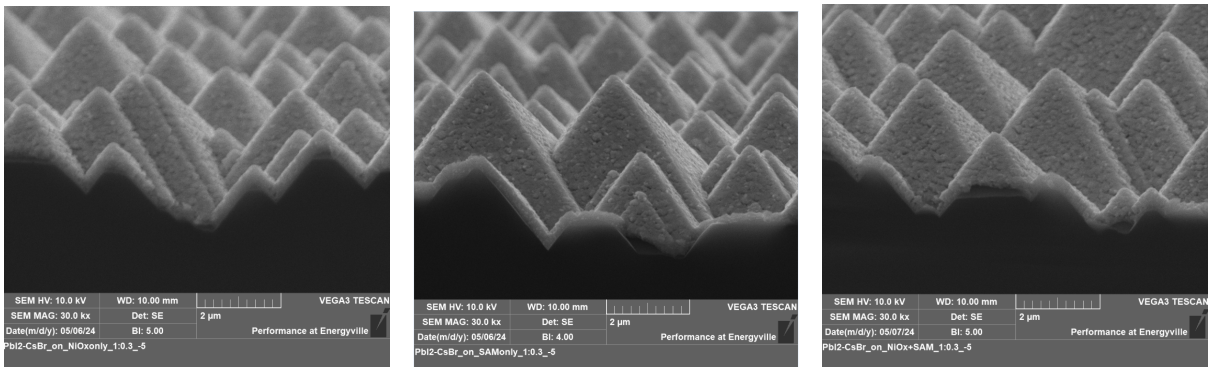

(a) PbI_2:CsBr on NiOx (b) PbI_2:CsBr on SAMs (c) PbI_2:CsBr on NiOx+SAMs

Figure 3.4: Cross-sectional scanning electron microscopy (SEM) images of co-evaporated PbI_2:CsBr (1:0.3 Å/s) on textured silicon substrate

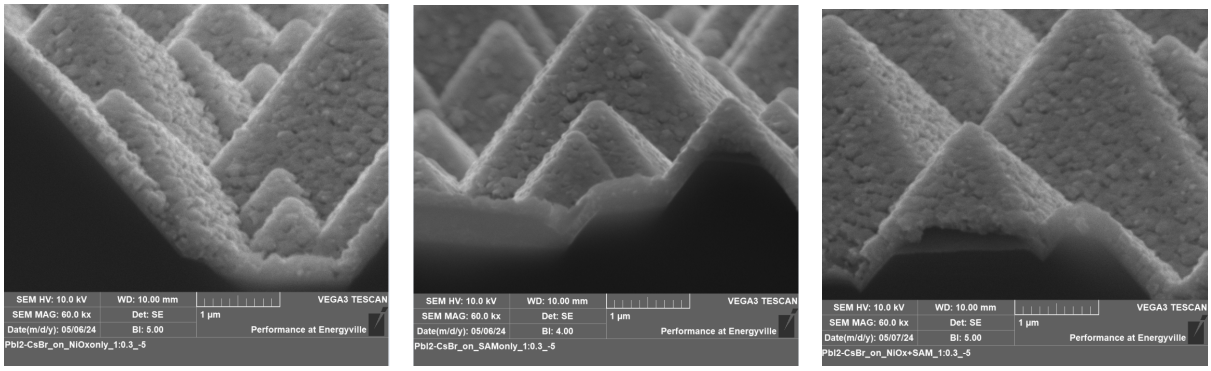

(a) PbI_2:CsBr on NiOX (b) PbI_2:CsBr on SAMs (c) PbI_2:CsBr on NiOx+SAMs

Figure 3.5: Zoomed-in SEM images of Figure 3.4

Under standard conditions, no significant differences were observed between the various evaporation configurations. However, the film deposited on NiOx appeared slightly rougher compared to the one on SAMs.

Two key parameters that could influence the outcome of the co-evaporation process are the substrate temperature and the evaporation rate. To investigate their effects, a series of experiments were carried out using evaporation rates of 4:1.2 Å/s at the reference temperature (- 5 °C) for PbI_2 and CsBr, respectively. These were compared to the standard deposition techniqueusing the rates of 1:0.3 Å/s. SEM imaging was used for characterisation. These adjustments were made to understand their effect on film morphology and material deposition.

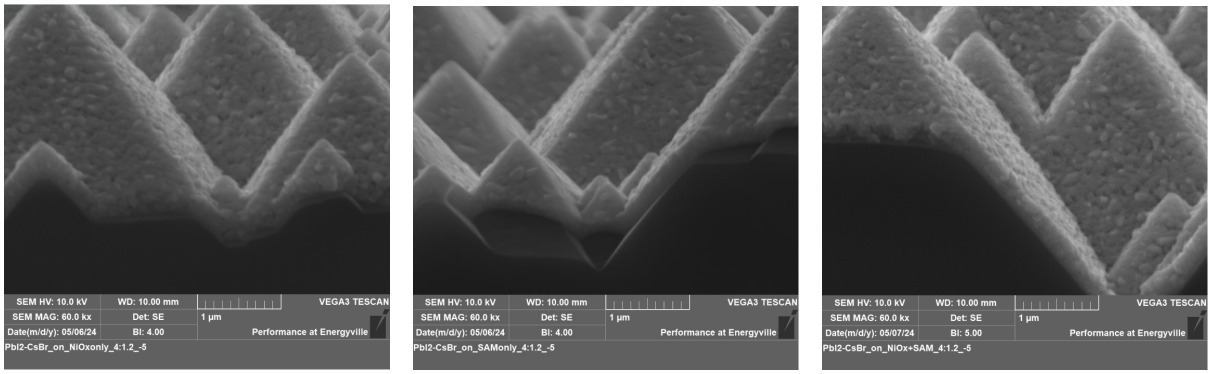

(a) PbI_2:CsBr on NiOX (b) PbI_2:CsBr on SAMs (c) PbI_2:CsBr on NiOx+SAMs

Figure 3.6: Cross-sectional SEM images of co-evaporated PbI_2:CsBr (4:1.2 Å/s) on textured silicon substrate.

The perovskite films that were evaporated with a higher deposition rate presented a smoother morphology with respect to the ones deposited using lower rates.

The focus then shifted to analysing the effect of substrate temperature on the deposition process. Since the film morphology showed no significant variation between the rates of 4-1.2 Å/s and 1-0.3 Å/s, an intermediate rate combination of 2-0.6 Å/s was selected for further investigation due to the reduce processing time. Both 30 °C and 60 °C substrate temperatures were evaluated to assess their effect on the film properties. No visible effects were caused by changing the substrate temperature.

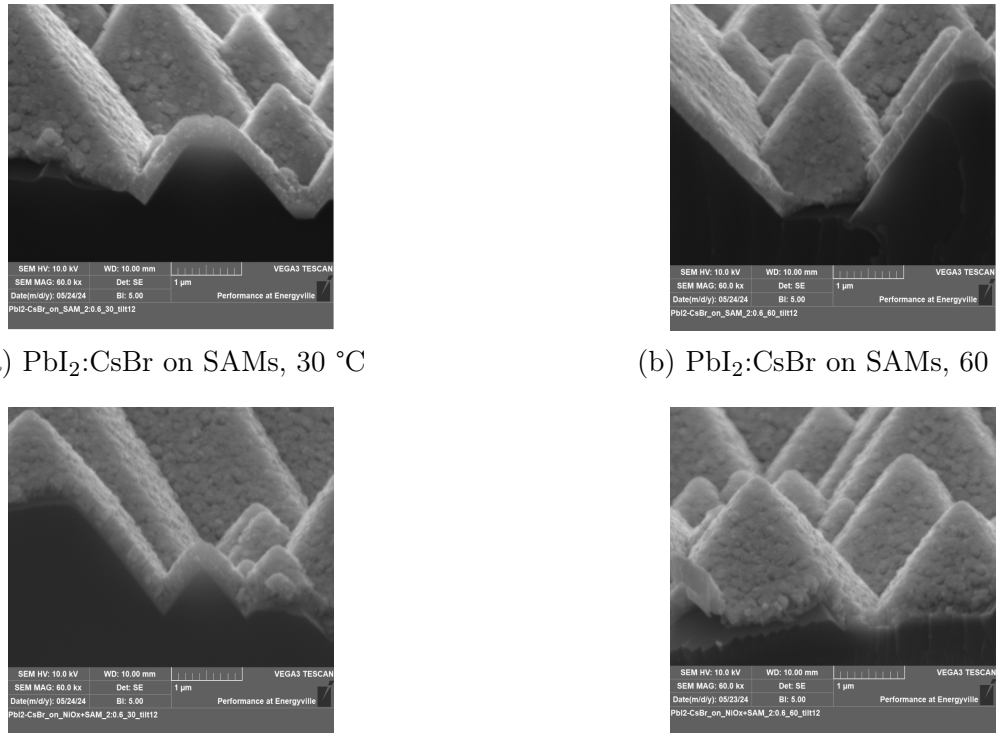

(a) PbI_2:CsBr on SAMs, 30 °C (b) PbI_2:CsBr on SAMs, 60 °C

(c) PbI_2:CsBr on NiOx+SAMs, 30 °C (d) PbI_2:CsBr on NiOx+SAMs, 60 °C

Figure 3.7: Cross-sectional SEM images of co-evaporated PbI_2:CsBr (2:0.6 Å/s) on textured silicon substrate. The substrate temperature was controlled at either 30 or 60 °C.

To gain a better understanding of the phenomenom, another evaporation was carried

out with the aim of understanding the role played by the ratio of PbI_2 to CsBr in a co-evaporation process. First, the extreme case of no CsBr in the evaporation process was investigated. The chosen rate was 2 Å/s PbI_2 and the chosen substrate temperature was -5 °C.

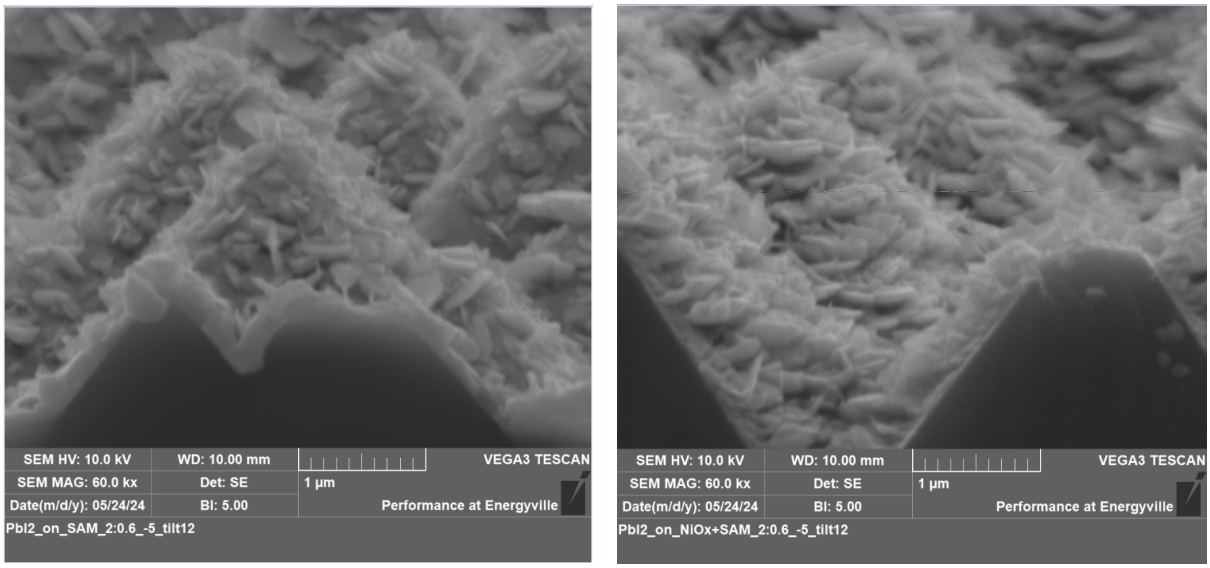

(a) PbI_2 on SAMs (b) PbI_2 on NiOx+SAMs

Figure 3.8: Cross-sectional SEM images of evaporated PbI_2 (2 Å/s) on textured silicon substrate. The substrate temperature was controlled at -5 °C.

The test showed a remarkable increase in porosity compared to the reference study (1:0.3 Å/s PbI_2:CsBr). This finding led to an adjustment of the CsBr content during the co-evaporation process to further increase the porosity and achieve deeper penetration of the organic solution in the second step of hybrid approach. To confirm this effect, a final test was conducted with the temperature still set at -5°C and the evaporation rate set to 1 Å/s for PbI_2 and 0.1 Å/s for CsBr. The results are shown in 3.9. It is clear that with a lower CsBr content in the co-evaporation step resulted in an increased porosity.

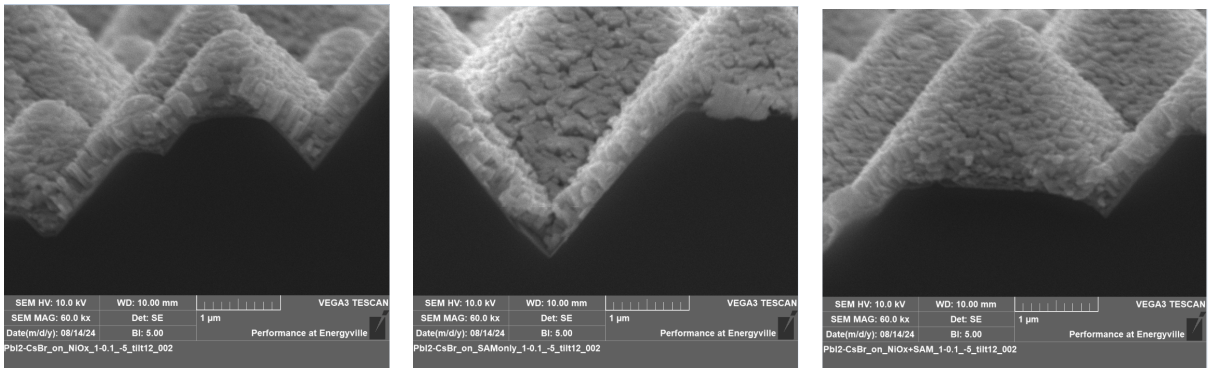

(a) PbI_2:CsBr on NiOx (b) PbI_2:CsBr on SAMs (c) PbI_2:CsBr on NiOx+SAMs

Figure 3.9: Cross-sectional SEM images of co-evaporated PbI_2:CsBr (1:0.1 Å/s) on textured silicon substrate. The substrate temperature was controlled at -5 °C.

3.4 Adjusting the organic solution composition

Changing the evaporation rate of the CsBr, but leaving the evaporation rate of the PbI_2 unchanged, necessitates adjustments to the concentration of organics in the solution. The aim of this series of experiments was to find the right iodine to bromine ratio in the organic solution to produce perovskite with the desired energy bandgap of 1.67 eV.

To find the optimal iodine-to-bromine ratio in the organic solution, single-junction perovskite solar cells were fabricated. A screening of five different ratios was conducted, followed by characterization using a solar simulator and analysis through steady-state photoluminescence (**SSPL**) and time-resolved PL (**TRPL**).

- **Solution 1**, 100 % FAI
- **Solution 2**, 100 % FABr
- **Solution 3**, ratio of 50% FAI and 50% FABr
- **Solution 4**, ratio of 40% FAI and 60% FABr
- **Solution 5**, ratio of 30% FAI and 70% FABr

The cells were fabricated using a standard fabrication process. After coating, the cells underwent standard ETL evaporation and metal contact deposition.

For characterisation, the solar simulator was used to evaluate the figure of merit of the cells and SSPL was used to evaluate the band gap obtained.

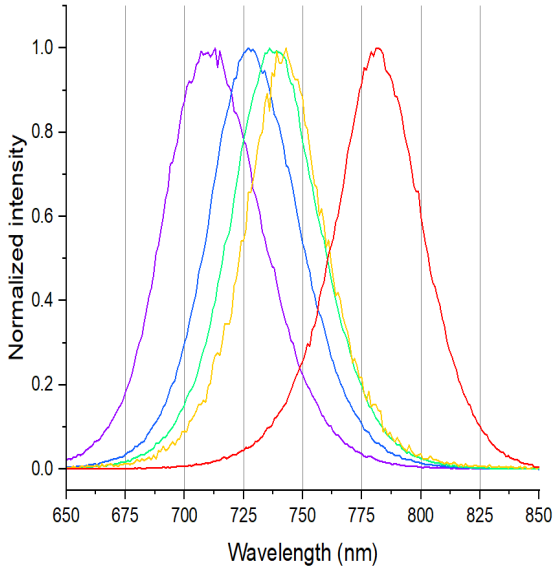

Figure 3.10: SSPL spectra of the investigated perovskite films.

- Solution 1, only FAI, a bandgap of 1.58 eV was measured from SSPL.
- Solution 2, only FABr, a bandgap of 1.75 eV was measured from SSPL.
- Solution 3, 50% FAI and 50% FABr, a bandgap of 1.67 eV was measured from SSPL.

- Solution 4, 40% FAI and 60% FABr, a bandgap of 1.68 eV was measured from SSPL.
- Solution 5, 30% FAI and 70% FABr, a bandgap of 1.71 eV was measured from SSPL.

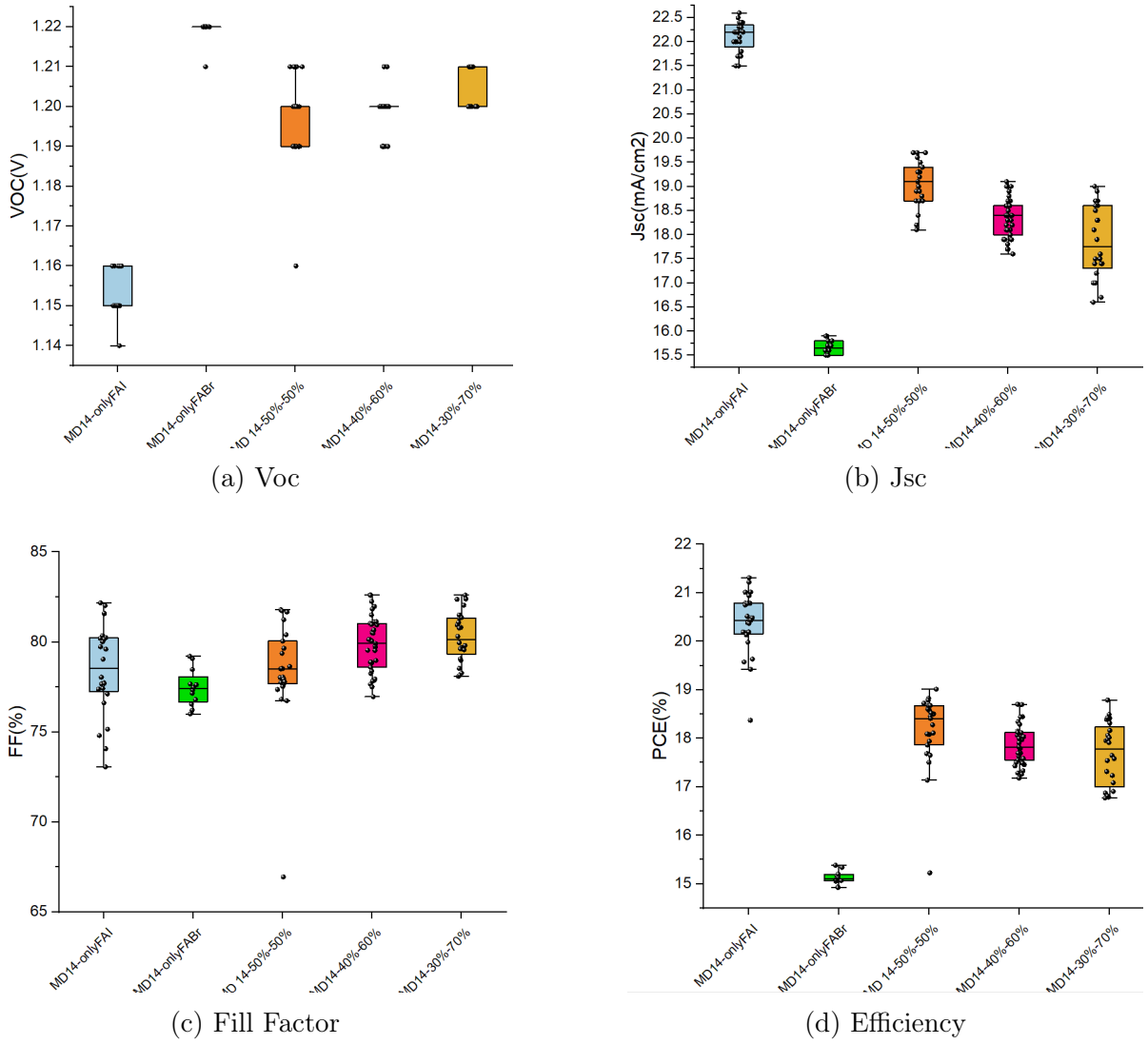

(a) Voc (b) Jsc

(c) Fill Factor (d) Efficiency

Figure 3.11: Color codes from left to right in each sub figure: only FAI, only FABr, 50/50, 40/60, 30/70 FAI/FABr ratios

From the solar simulator analysis presented in Figure 3.11, it is evident that as the bandgap decreases, the Voc (Figure 3.11a) also decreases, while the Jsc exhibits the opposite trend, increasing as the bandgap decreases (Figure 3.11b).

To achieve better-performing cells, it is crucial that each layer of the cell stack is optimized for performance. As a standard fabrication process, SAMs have been deposited using spin-coating followed by ethanol rinsing. However, recent studies have highlighted the benefits of using thermal evaporation for depositing SAMs instead of spin-coating, citing improvements in efficiency and Voc.[33]

The aim of this experiment was to compare single junction perovskite solar cells realised with spin-coated Me-4PACz versus those fabricated with evaporated Me-4PACz.

After cleaning the substrates, NiOx was deposited through DC sputtering, followed by annealing at 300 °C in air. Half of the samples had thermally evaporated SAMs, the other half had spin-coated SAMs. This was followed by co-evaporation of PbI_2 and CsBr, spin-coating of the organics, annealing at 130 °C, thermal evaporation of the ETL (LiF/C60/BCP), and finally thermal evaporation of the silver contacts.

To characterise the cells, standard measurements were conducted with the solar simulator to extract the main photovoltaic parameters of the cells. Unfortunately some spin-coated samples were damaged by handling mistake, resulting in fewer data points for this condition, but it was still possible to see a trend.

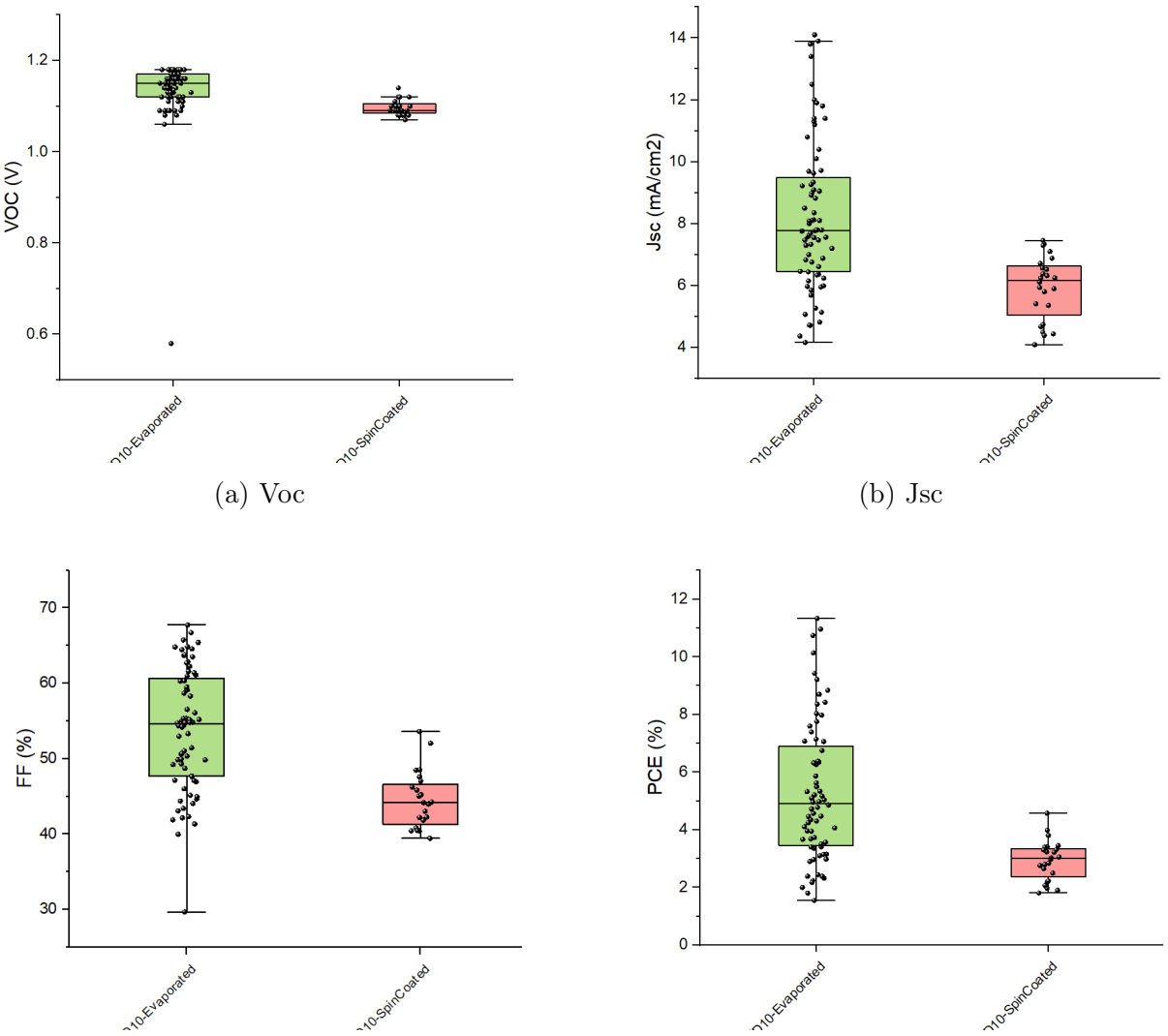

(a) Voc (b) Jsc

(c) Fill factor (d) Efficiency

Figure 3.12: Green: evaporated SAMs, Pink: spincoated

Comparing the JV curves, it is clear that evaporated SAMs resulted better cells performance in all the parameters including Voc, Jsc and PCE, despite that the performance for all the cells presented here are only moderate, indicating large room for further processing optimization, which will be discussed in the following sections.

3.5 Bulk and surface modification

The PSCs still show large room for improvement. The average efficiency obtained is still low, mainly due to Jsc and FF losses. Another general challenge for wide bandgap perovskite, which has not been intensively discussed yet in this work, is the instability due to phase segregation under illumination. t has been reported that bulk and surface passivation passivate the defects, thus enhancing both initial efficiency and stability. Without such defect passivation, the defects can create energy states within the energy bandgap that trap charge carriers and promote degradation, for example, by reaction with ambient moisture and oxygen, and facilitate ion migration. [20]

To reduce the defect density, several techniques have been explored. It is usually done by using additives, also often referred to as bulk passivators. These materials can be either added to the precursor itself or be added in a subsequent step onto the as-prepared (wet) perovskite films.

Not only passivators reduce the number of defects, they can also form physical barriers against different degrading agents, such as moisture and oxygen. In addition, they can improve charge extraction at the interface between the perovskite and the charge transport layer. [20]

3.5.1 Bulk modification

Recently, two different materials, 2,3,4,5,6-pentafluorobenzylphosphonic acid (**pFBPA**) and 1-(phenylsulfonyl)pyrrole (**PSP**), have been reported as bulk additives in the literature. Such additives aimed to improve the crystalline quality of the perovskite film using these additives, the realized perovskite had an energy bangap of 1.67 eV.

pFBPA

Figure 3.13: pFBPA molecule

The first bulk additive selected for this study was 2,3,4,5,6-pentafluorobenzylphosphonic acid (pFBPA).

According to Chin et al. [27], X-ray photoelectron spectroscopy (XPS) revealed that this bulk additive interacts with the Pb_2+/Pb0 surface defects. The phosphonic group of FBPAc binds to the lead-related defects in the material, reducing the number of non-radiative recombination states at the top surface of the material. Additionally, they also concluded that the use of the bulk additive helps to reduce stress losses at the perovskite/ETL interface and helps to achieve larger domains in the perovskite structure

itself. In the referenced study, [27] they used a pFBPA stock solution concentration of 5 mM (around 1.3 mg/mL) dissolved in ethanol and then added directly to the powders. A very similar approach was used in this work: a stock solution of 2 mg/mL dissolved in ethanol was either added directly to the powders or further diluted with ethanol to achieve the desired concentration of pFBPA.

The first concentration screening involved 3 concentrations:0.5, 1.3 and 2 mg/mL.

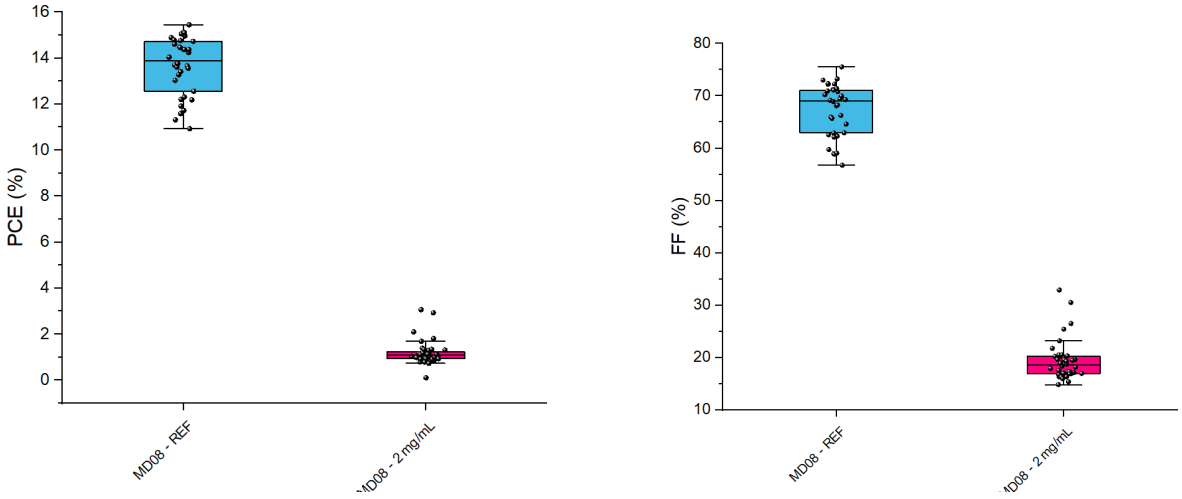

(a) Efficiency (b) Fill Factor

Figure 3.14: Comparison between reference cells and cells with a high concentration of pFBPA

From this initial screening, as can be seen in Fig. 3.14, it is evident that too high a concentration of bulk additive can be counterproductive; the comparison shows that the reference cells (i.e. realised without bulk additive) have a better fill factor and a better efficiency than the cells with a high concentration of bulk additive.

The focus then shifted to lower concentrations of pFBPA, and 0.1, 0.15 and 0.2 mg/mL were screened.

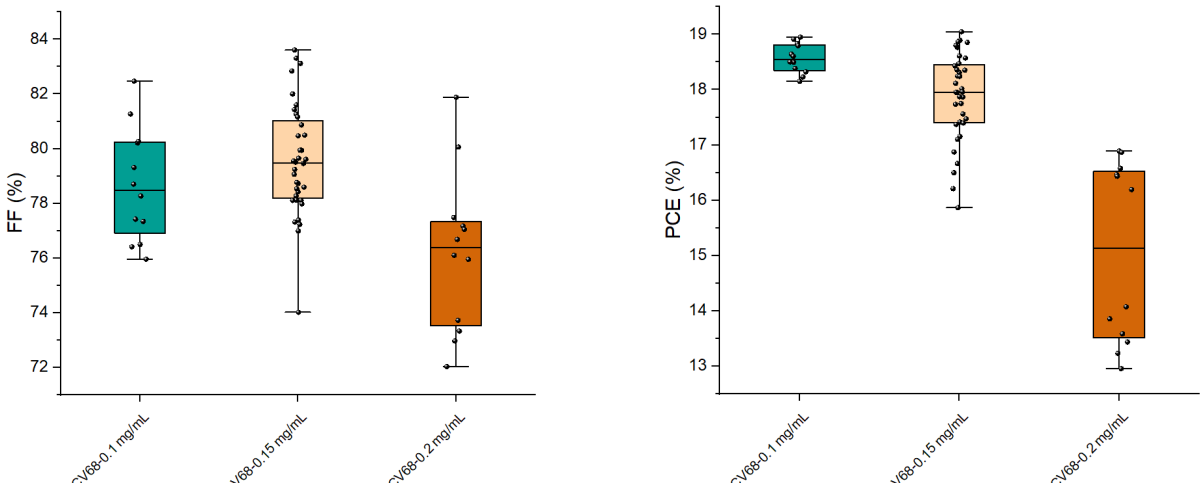

(a) Fill factor (b) Efficiency

Figure 3.15: Color codes from left to right in each sub figure, 0.1, 0.15, 0.2 (mg/ml)

From this further analysis, as shown in Fig. 3.15, we concluded that a lower concentration of pFBPA yields better performances.

Further tests were conducted using a solar simulator to evaluate the response of the cells to **light soaking**. Each cell was subjected to continuous light exposure and measured every minute during 10-minutes exposure. Figure 3.16 presents a comparison between the first and last measurements for each sample. Unfortunately, these tests revealed instability associated with light soaking.

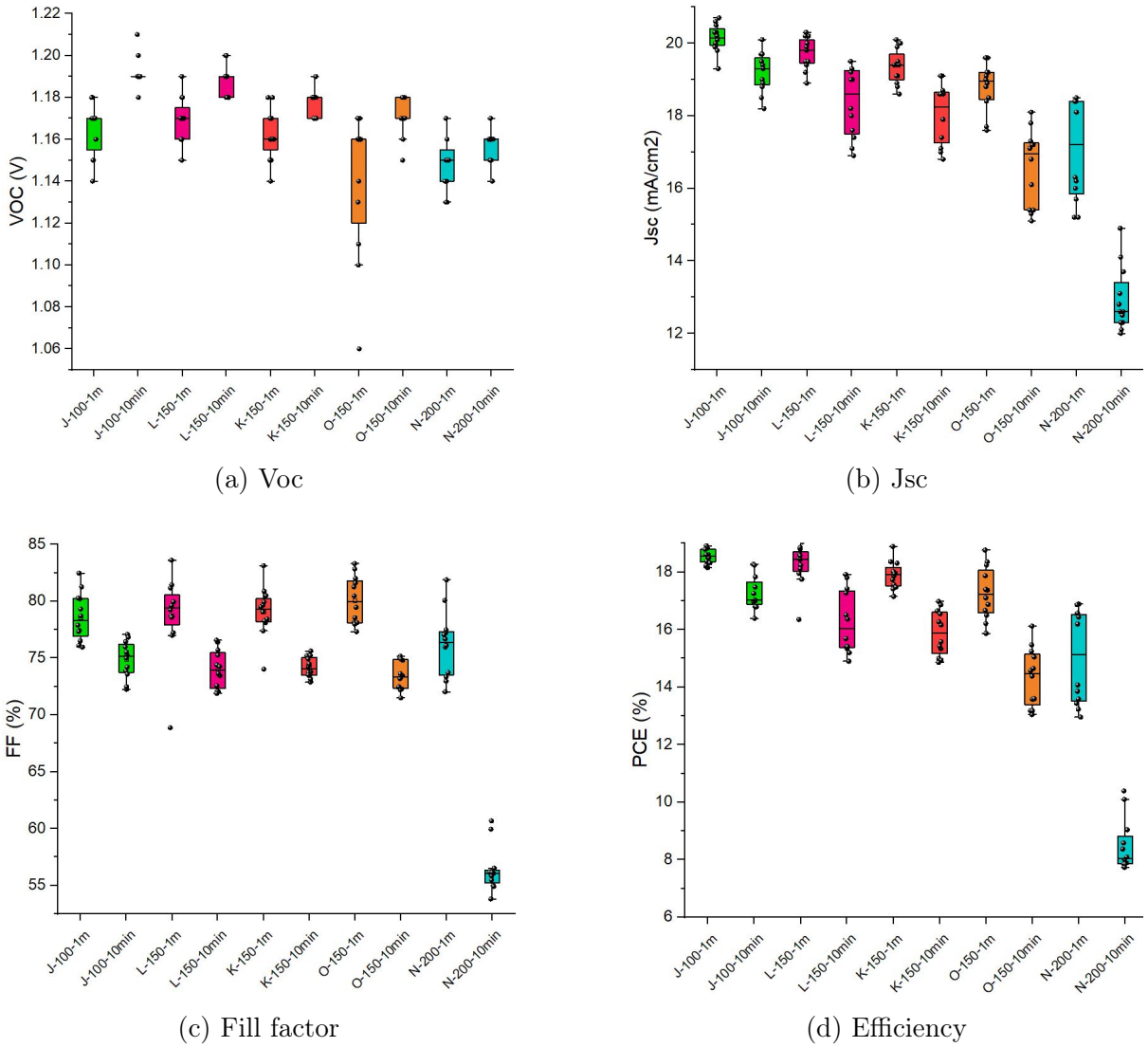

(a) Voc

(b) Jsc

(c) Fill factor

(d) Efficiency

Figure 3.16: Color codes from left to right in each sub figure, 0.1, 0.15, 0.15, 0.2 (mg/ml)

While the Voc (3.16a) shows improvement with lightsoaking, the FF (3.16c), the efficiency (3.16d) and Jsc (3.16b) showed decline. Therefore we conclude that the pFBPA is detrimental to the light stability of the PSCs.

PSP

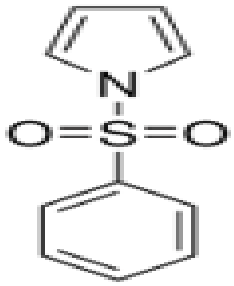

Figure 3.17: PSP molecule

Following the investigation of pFBPA and its effects on device performance, the study was extended to investigate another potential bulk additive, 1-(phenylsulfonyl)pyrrole (PSP). According to [34], PSP exhibits a passivating effect, leading to improvements in efficiency and a significant increase in fill factor. In addition, PSP was found to increase the Voc, which is consistent with a reduction in trap density.

Similarly as the pFBPA experimental approach, a stock solution of 2 mg/mL was realized, and depending on the desired concentration of PSP, it was either directly added to the solution or diluted with additional ethanol.

The first screening focused on the following concentrations: 0.5, 1 and 2 mg/mL.

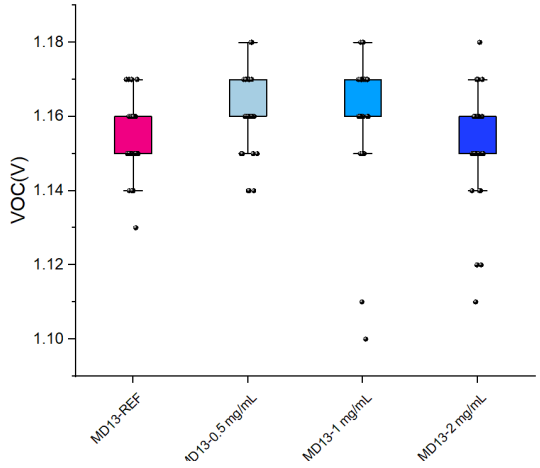

(a) Voc

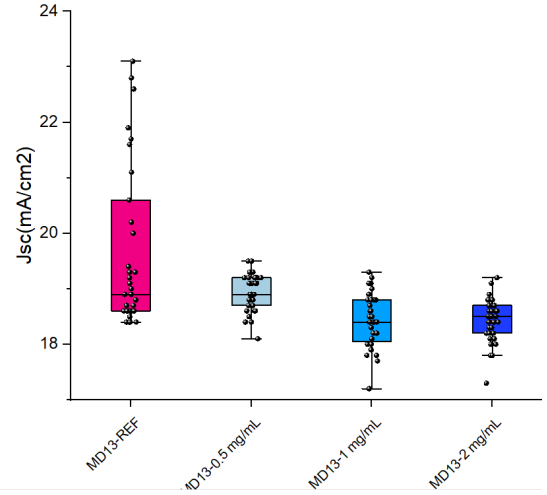

(b) Jsc

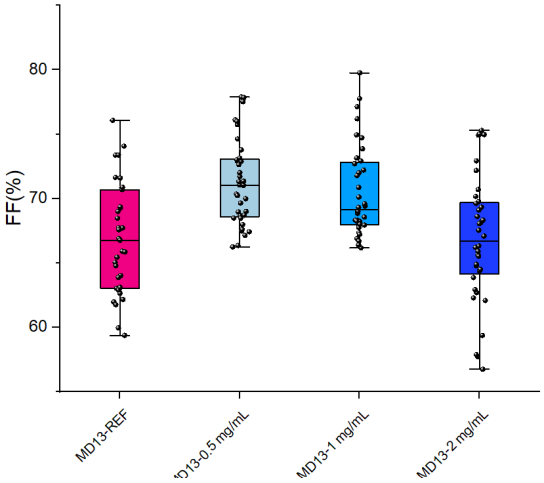

(c) Fill factor

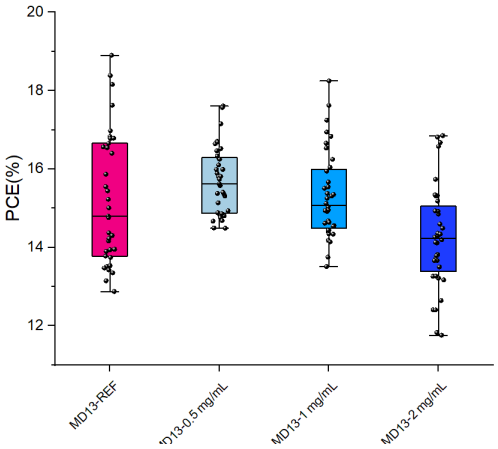

(d) Efficiency

Figure 3.18: Color codes from left to right in each sub figure, ref, 0.5, 1, 2 (mg/mL)

Similarly to pFBPA, lower concentrations of the bulk additive PSP also resulted in better performance. Consequently, the next screening focused on lower concentrations: 0.1, 0.25 and 0.5 mg/mL.

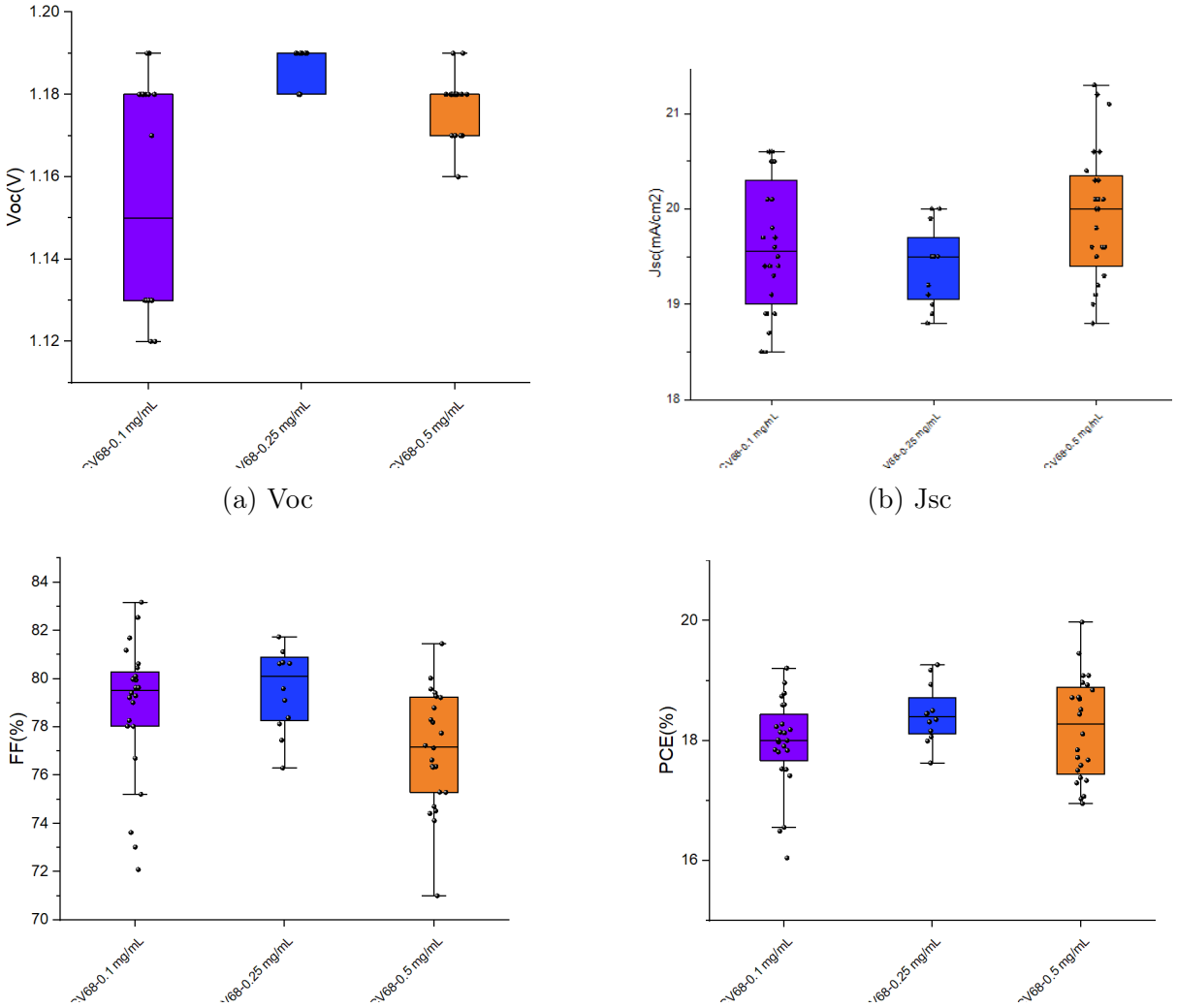

(a) Voc (b) Jsc

(c) Fill factor (d) Efficiency

Figure 3.19: Color codes from left to right in each sub figure, 0.1, 0.25, 0.5 (mg/mL)

The study demonstrated that the optimal concentration is indeed the range between 0.1 mg/mL and 0.5 mg/mL. Further characterization was carried out to ensure that the cells treated with PSP do not suffer from light soaking instability, as observed with pFBPA. The chosen concentration for this batch was 0.5 mg/mL.

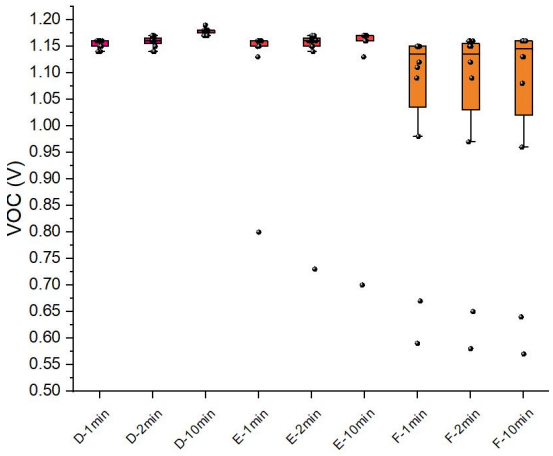

(a) Voc

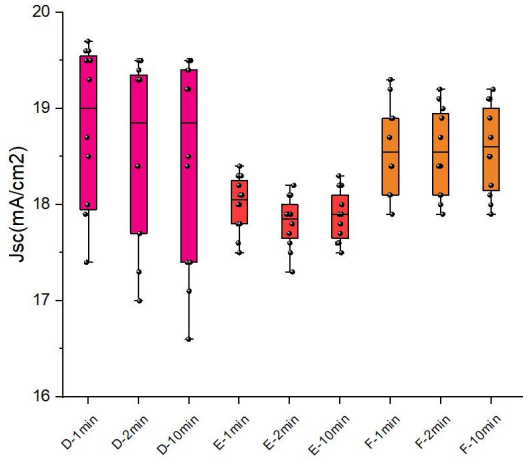

(b) Jsc

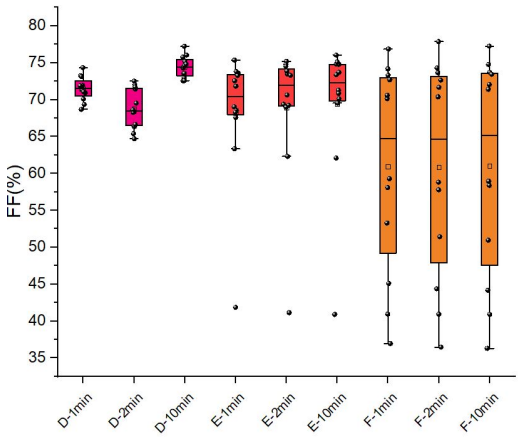

(c) Fill factor

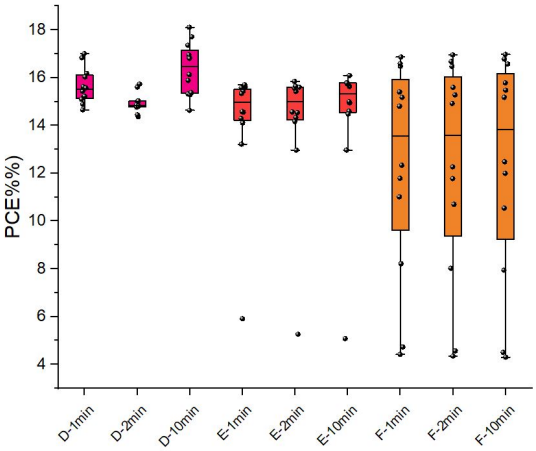

(d) Efficiency

Figure 3.20: Comparison between measures under light soaking condition for 0.5 mg/mL concentration, at 1 mintute, 2 minutes, and 10 minutes.

For the pFBPA, a light soaking analysis was also conducted for the PSP samples. The samples were subjected to continuous light exposure for 10 minutes. In Figure 3.20, different samples treated with 0.5 mg/mL of PSP as a bulk additive were analyzed. The figure shows a comparison between measurements taken after 1 minute, 2 minutes, and 10 minutes of light exposure. From this analysis, it can be concluded that PSP demonstrates greater stability compared to pFBPA and does not exhibit the same light-soaking instability.

3.5.2 Surface modification

The aim of these experiments was to achieve better performances by modifying the surface of the perovskite layer through a surface treatment by spin-coating a solution containing the passivator onto the perovskite surface. The fabrication steps for these experiments follow the standard fabrication process until the perovskite is annealed, then the surface passivator is spin-coated onto the perovskite, followed by a short annealing step. Then the steps of the standard process continue.

The chosen evaporation rate for PbI_2 and CsBr was 1:0.1 Å/s, with the aim of achieving 230 nm and 23 nm respectively.

PI

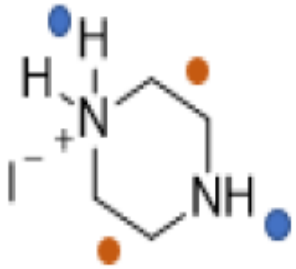

Figure 3.21: PI molecule

Using piperazinium iodide (PI) as a surface treatment, [35] it was showed that the main effect of PI was not a chemical passivation of the perovskite surface, i.e. it doesn't reduce the defects of the perovskite, but reduce of the energy offset between the conduction band (CB) and the lowest unoccupied molecular orbital. This allowed the quasi-Fermi level of the electrons to be closer to the edge of the perovskite CB. [36] In terms of device performance, the surface treatment resulted in a significantly higher Voc.

As for the experimental approach, a stock solution of 2 mg/mL was prepared with the aim of diluting it and obtaining different concentrations to be able to carry out a concentration screening. To obtain the stock solution, the PI was diluted with 2-propanol in an inert atmosphere. Stirring didn't result in proper dissolution of the PI in 2-propanol, so the solution was further diluted and sonication at 65 °C for one hour was used to improve dissolution.

The concentrations of PI for the screening chosen to be confronted with the reference cells were: 0.1, 0.3 and 0.5 mg/mL. The solution was spin-coated atop annealed perovskite at 4500 rpm for 30 sec, then the samples were annealed for 5 min at 100 °C in an inert atmosphere.

As for the used ETL stack, since in the literature it was claimed to have better performance without the LiF interface, [36] half of them were realized with the classic ETL stack (LiF/C60/BCP), while the other half was realized without the LiF layer (C60/BCP).

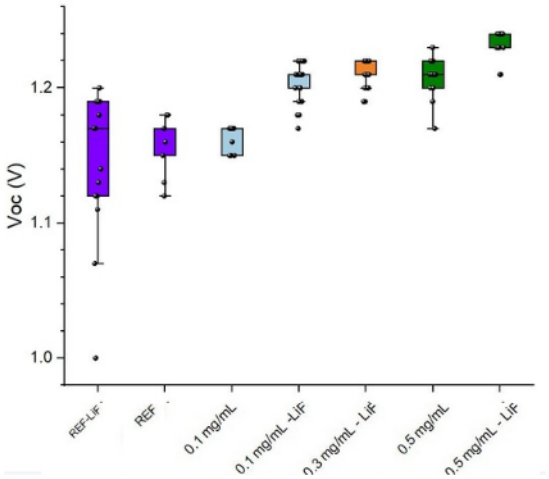

(a) Voc

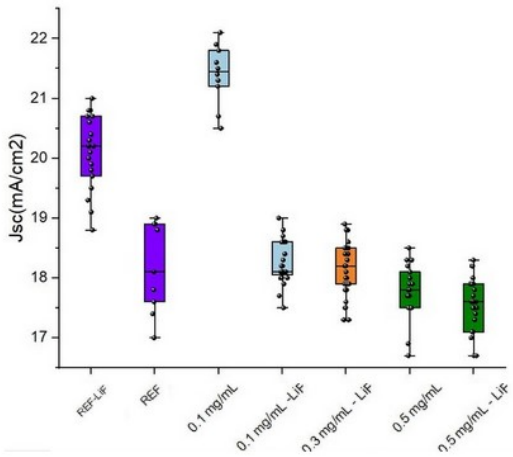

(b) Jsc

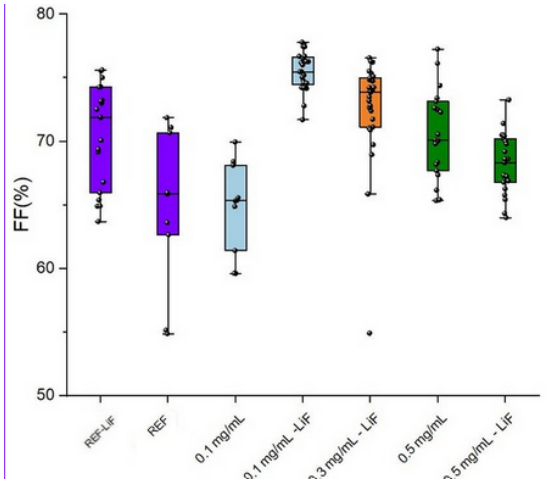

(c) Fill factor

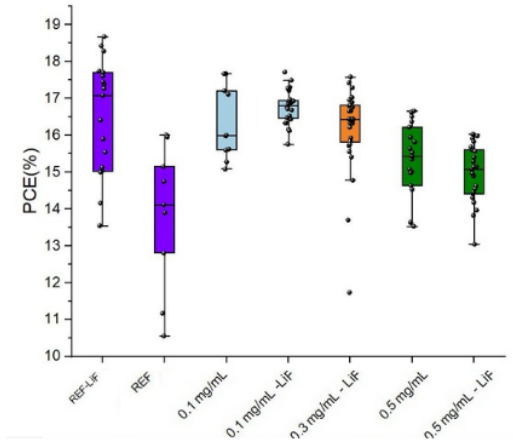

(d) Efficiency

Figure 3.22: Color codes from left to right in each sub figure, ref, 0.1, 0.3, 0.5 (mg/mL)

As can be seen in Fig. 3.22a and 3.22c, the Voc and FF show an increase after the surface passivation treatment, the efficiency is comparable with that of the reference cells, while the Jsc shows a little decrease. Contrary on what [36] rescontrated, the use of PI does not substitute the application of LiF.

DMPESI

Suo et al. [37], used dimethylphenethylsulfonium iodide (DMPESI) as a surface treatment for one-step perovskite deposition. They observed a passivation effect on surface defects, a prolongation of the charge-carrier lifetime, and the suppression of non-radiative recombination. These benefits contributed to improved PSC performance, including higher efficiency and increased stability under light soaking. [37] In this project, the concentrations of DMPESI for the screening chosen to be confronted with the reference cells were: 0.5 and 1 mg/mL.

The DMPESI solutions were spin-coated onto the annealed perovskite at 4500 rpm for 30 sec, then the samples were annealed for 5 min at 100 °C in an inert atmosphere.

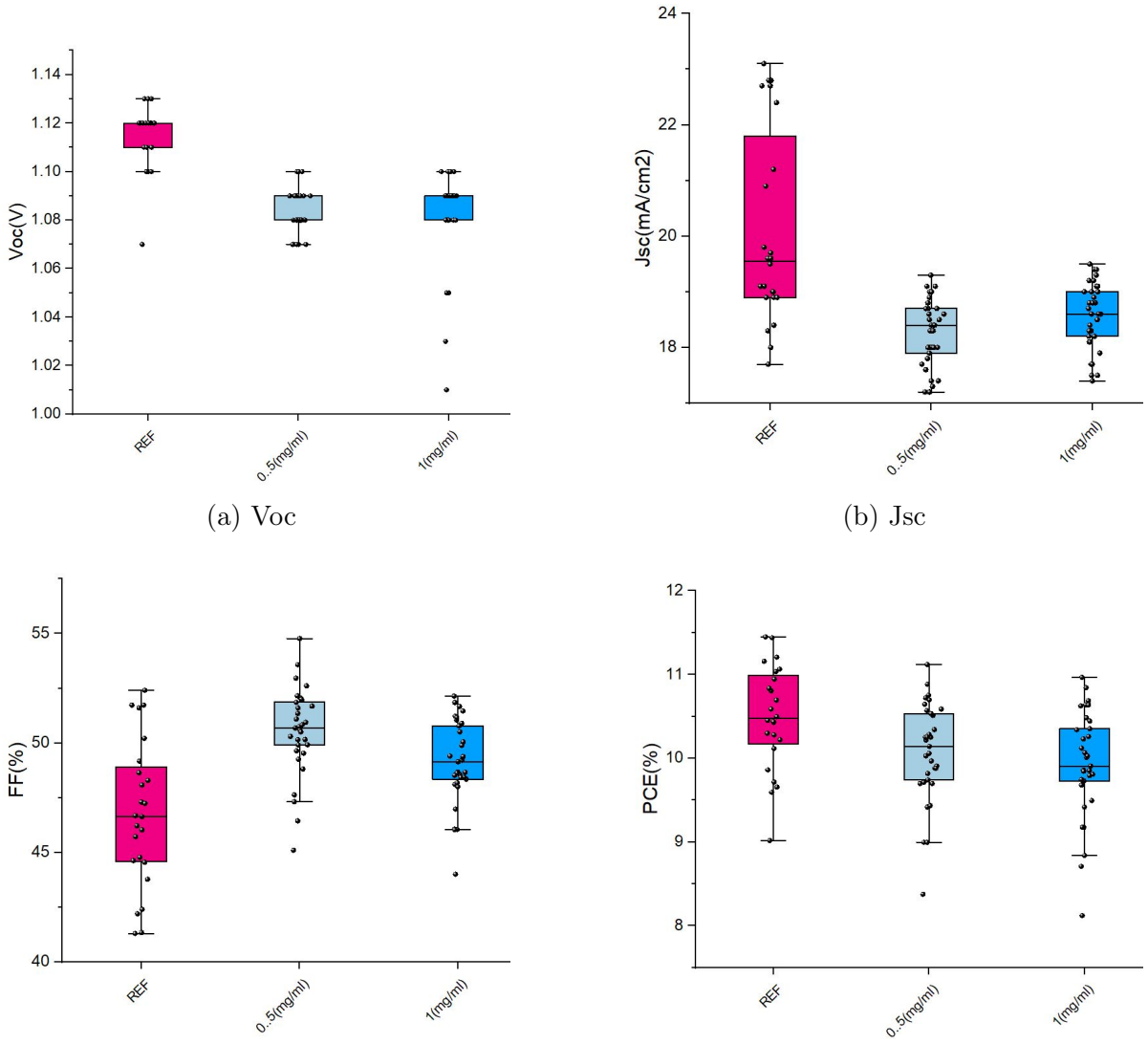

(a) Voc

(b) Jsc

(c) Fill factor

(d) Efficiency

Figure 3.23: Color codes from left to right in each sub figure, ref, 0.5, 1 (mg/mL)

As shown in Fig. 3.23, the use of the surface treatment, in this run, except for a slight increase in the FF, showed overall no benefits with respect to the reference cells. The Voc was impacted even negatively.

$PDAI_2$

Hu et al. [38] reported that by using 1,3-propane-diammonium iodide ($PDAI_2$) as surface treatementm they were able to realise perovskite films that showed apparently larger grain sizes. They also identified higher Voc and efficiency. Similarly both PI and DMPESI, the solution of $PDAI_2$ was spin-coated onto the annealed perovskite at 4500 rpm for 30 sec, then the samples were annealed for 5 min at 100 °C in an inert atmosphere.

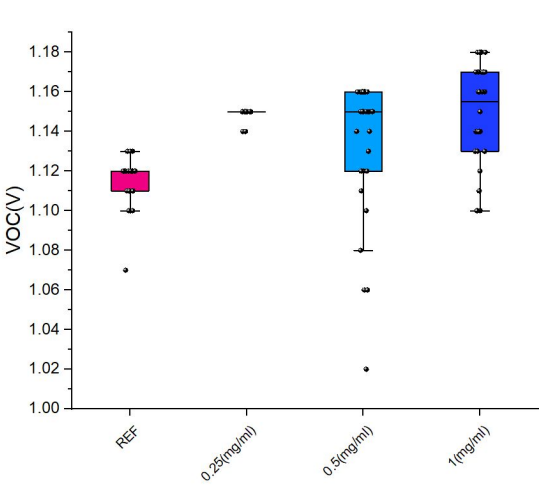

(a) Voc

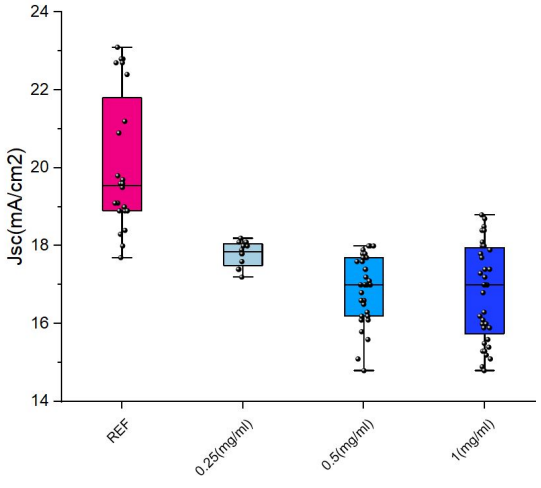

(b) Jsc

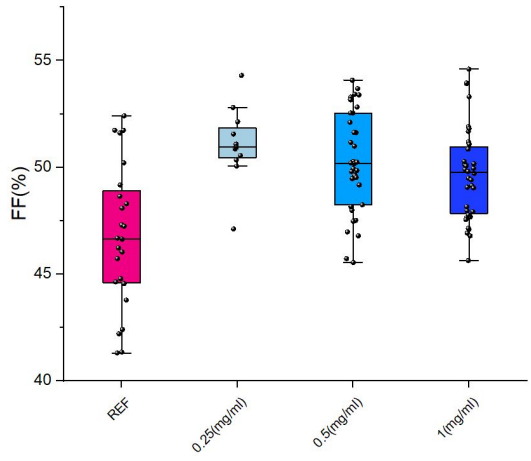

(c) Fill factor

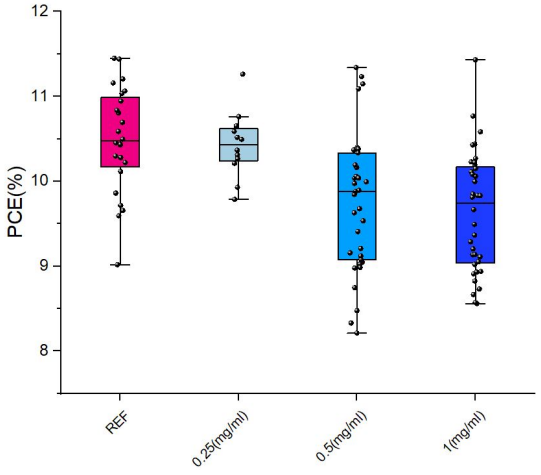

(d) Efficiency

Figure 3.24: Color codes from left to right in each sub figure, ref, 0.25, 0.5, 1 (mg/mL)

As shown in Fig. 3.24, the $PDAI_2$ induced a slight increase in the FF and in the Voc, unfortunately the efficiency and Jsc didn't have the same improvement.

3.6 Conclusion

In this chapter, the impact of a high annealing temperature on silicon heterojunction cells was investigated, concluding that 300°C was too high for optimal performance. Additionally, a morphology study showed the benefits of using a lower evaporation rate for PbI_2 with a ratio of 1:0.1 Å/s.

Regarding the materials tested, pFBPA exhibited significant potential but lacked stability under light soaking conditions, while PSP showed greater potential overall. Surface treatments were also examined: PI treatment resulted in an increase in the open-circuit voltage (Vocm), especially at the highest concentration of 0.5 mg/mL. Conversely, DMPESI did not provide any improvement compared to the reference cell, while $PDAI_2$ led to a slight increase in both fill factor (FF) and Voc.

Chapter 4

Conclusion and Outlook

In this study, bulk- and interface-modification treatments were applied to enhance the performance of 1.67 eV perovskite solar cells. These treatments, aimed at modifying the bulk and surface of the perovskite layers, showed promising results, particularly in improving the open-circuit voltage. However, there is still large room for improvement. An optimal concentration range was identified for each treatment: for pFBPA, the optimal concentration lies between 0.05 mg/mL and 0.1 mg/mL, while for PSP, it is between 0.1 mg/mL and 0.5 mg/mL. Unfortunately, reproducibility issues between batches make it difficult to define a definitive optimal condition. Further characterization is required to fully understand the effects of these treatments on the perovskite material.

Regarding **bulk modification**, the additive showed great potential. The **pFBPA** additive yielded significant results, including a notable increase in Voc (1.25 V), but unfortunately exhibited poor light-soaking stability. Further investigation is required. On the other hand, the **PSP** additive demonstrated better light-soaking stability of the fabricated perovskite compared to pFBPA.

Regarding the **surface treatments**, **DMPESI** at lower concentration of 0.5 mg/mL showed an improvement in the fill factor (FF) of the cells, suggesting that a lower concentration is necessary to achieve positive results from this treatment. On the other hand, **$PDAI_2$** led to enhancements in both Voc and FF but had a negative impact on Jsc, indicating the need for additional testing and characterization. The **PI** treatment showed promising results, with a significant increase in Voc (1.25 V); however, the FF did not reflect a similar improvement. Further investigation is necessary to fully understand the impact of these treatments.

The morphology study on silicon solar cells confirmed that an evaporation rate of 1-0.1 Å/s (PbI_2:CsBr) results in a more porous structure in the first scaffold layer compared to 1-0.3 Å/s (PbI_2:CsBr), which is beneficial to a better perovskite formation. Due to this change in evaporation rate, the solution ratio had to be adjusted, and the optimal ratio for achieving a bandgap of 1.67 eV was identified.

To achieve reproducible results further research is necessary, especially studies on the interaction between different additives and the perovskite layer itself.

Future work should focus on employing additional characterization techniques, such as X-ray diffraction, Grazing-Incident Wide-Angle X-Ray Scattering (GIWAXS), and high-resolution scanning electron microscopy, to gain deeper insights into the underlying mechanisms in the bulk and at the surface of treated perovskite at play. Additionally, Quasi-Fermi Level Splitting (QFLS) studies will be invaluable for assessing the electronic quality of perovskite layers and identifying non-radiative recombination losses. These

insights will be crucial for translating the results from single-junction solar cells to high efficiency perovskite/silicon tandem solar cells.

Ringraziamenti

Grazie a me prima di tutto. Per tutti gli altri, le parole non esprimeranno mai a pieno cosa provo in questo momento, ma come sempre, ci proviamo, e come viene , così ce la prendiamo.

This thesis would not have existed without the help of my supervisors, and all the other amazing people who assisted me in the lab through my many doubts and visible mistakes. Thank you.

All of this would not have been possible also without the support of my many companions in this adventure.

Le sciure, my chosen family. Chiara, un rapporto costellato di drammi e battibecchi costanti, per aver fatto vincere la noia, grazie. Vale, the caregiver, per essere mia amica e prenderti sempre cura di me, grazie. Vero, nonostante i vari tentativi di omicidio, nonostante come siano andate le cose con Jenna e Alexander, per essere la mia parte razionale, grazie. Geppi, l'amore non è bello se non è litigarello, e il nostro è tanto litigarello, per essere sempre disponibile a ricominciare da capo, grazie. France, per aver reso i giorni pesanti più leggeri, grazie.

Svizzero, Obi-Ewan-Kenobi, Cipriano, for being by my side no matter what, without asking questions, pushing me to do better, thank you.

Itram, sempre al mio fianco, la mia psicologa personale, le parole non basteranno mai ad esprimere la mia gratitudine nei tuoi confronti, in fondo non sono neanche mai servite, grazie.

Martina, Sofia, Vera, ormai sono più gli anni che abbiamo passato insieme che quelli in cui non ci conoscevamo, per non avermi mai lasciato, per essere cresciute con me, grazie.

Mamma e papà, per avermi dato tutto, grazie.

Armando e Matteo, per aver condiviso con me la vostra infanzia, i traumi, le gioie, grazie.

Marco, per avermi spinto a chiedere aiuto quando necessario, per essere stato l'aiuto di cui avevo bisogno, grazie.

Valentina, per esserci stata da quando abbiamo iniziato questo percorso, grazie.

Deni, per essere mia sorella, grazie.

Ai ragazzi di Unisa, distanti ma mai lontani.

To all the nanotech out there, because we are a family, we are Nanofam

Bibliography

[1] International Energy Agency. Renewables 2023: Executive summary, 2023.

[2] Mathieu Leduc, Alexander J. Smith, Ravi Patel, Pavan Kumar, and Ling Zhao. Semiconductors for next-generation electronics and optoelectronics: A review. *Cell Reports Physical Science*, 5(8):101123, 2024.

[3] Penn State College of Earth and Mineral Sciences. Solar simulators. `https://www.e-education.psu.edu/meteo300/node/683`.

[4] PVEducation.org. Air mass. `https://www.pveducation.org/pvcdrom/properties-of-sunlight/air-mass`.

[5] U.S. Energy Information Administration. Photovoltaics and electricity, 2024.

[6] Author Unknown. Solar cell technology. In *Handbook of Solar Cells*. Oxford University Press, 2024.

[7] U.S. Department of Energy. Solar photovoltaic cell basics, 2024.

[8] PVEducation. Solar cell structure, 2024.

[9] Nitin Patil, Shijun Liao, and Shashank Priya. *Perovskite Photovoltaics: Fundamentals and Future Directions*, chapter 1, pages 1–26. Elsevier, 2023.

[10] PV Education. I-v curve. `https://www.pveducation.org/pvcdrom/solar-cell-operation/iv-curve`. Accessed: 2024-08-06.

[11] PV Education. Quantum efficiency.

[12] William Shockley and Hans J. Queisser. Detailed balance limit of efficiency of p-n junction solar cells. *Journal of Applied Physics*, 1961.

[13] Maksym Baijum, Adil Yarema. Recent advances in solar energy conversion and photovoltaic technologies. *Frontiers in Energy Research*, 2022.

[14] University of Cambridge DoITPoMS. Direct and indirect band gaps, 2024.

[15] Encyclopaedia Britannica. Thin-film solar cell, 2024.

[16] National Renewable Energy Laboratory (NREL). Best research-cell efficiency chart, 2024.

[17] Quinten Akkerman and Manna Liberato. Nanomaterials for photovoltaic applications: An overview. *Frontiers in Chemistry*, 2020.

[18] Qi Jiang and Kai Zhu. Rapid advances enabling high-performance inverted perovskite solar cells. *Nature Reviews Materials*, 2024.

[19] ScienceDirect. Perovskite. `https://www.sciencedirect.com/topics/earth-and-planetary-sciences/perovskite`.

[20] Wei et al. Zhang. Tailoring passivators for highly efficient and stable perovskite solar cells. *Journal of Solar Energy*, 2023.

[21] PV Education. Tandem cells, 2024.

[22] Matteo cocuzza. Corso di physics of technological process. Online, 2022/2023. Materiale didattico, Politecnico di Torino.

[23] Yi-Yang Peng, Shruti Srinivas, and Ravin Narain. Modification of polymers. In *Polymer Science and Nanotechnology: Fundamentals and Applications*. Elsevier, 2020.

[24] Zijun Yi and Xin et al. Li. Self-assembled monolayers (sams) in inverted perovskite solar cells and their tandem photovoltaics application. *InfoMat*, feb 2024.

[25] ScienceDirect. Thermal evaporation. `https://www.sciencedirect.com/topics/chemistry/thermal-evaporation#related-terms`.

[26] Junghwan Lee, Dong Hoe Kim, Min Su Kim, and Nam-Gyu Park. Multi-component alloys for stable and efficient perovskite solar cells. *Joule*, 2023.

[27] Xin Yu et al. Chin. Interface passivation for 31.25%-efficient perovskite/silicon tandem solar cells. *Science*, 2023.

[28] PV Education. Measurement of solar cell efficiency, 2024.

[29] Sinovoltaics. Standard test conditions (stc): Definition and problems, 2024.

[30] NanoScience Instruments. Scanning electron microscopy. `https://www.nanoscience.com/techniques/scanning-electron-microscopy/`, 2024.

[31] Science Education Resource Center (SERC). Scanning electron microscopy (sem), n.d.

[32] LibreTexts. Photoluminescence, phosphorescence, and fluorescence spectroscopy, 2024.

[33] Ahmed Farag and Thomas et al. Feeney. Evaporated self-assembled monolayer hole transport layers: Lossless interfaces in p-i-n perovskite solar cells. *Advanced Energy Materials*, 2023.

[34] Zheng Liang and Yong et al. Zhang. Homogenizing out-of-plane cation composition in perovskite solar cells. *Nature*, 2023.

[35] Fengzhu Li, Xiang Deng, Feng Qi, Zhen Li, Danjun Liu, Dong Shen, Minchao Qin, Shengfan Wu, Francis Lin, Sei-Hum Jang, Jie Zhang, Xinhui Lu, Dangyuan Lei, Chun-Sing Lee, Zonglong Zhu, and Alex K.-Y. Jen. Regulating surface termination for efficient inverted perovskite solar cells with greater than 23% efficiency. *Journal of the American Chemical Society*, 142(51):21656–21665, 2020.

[36] et al. Mariotti. Interface engineering for high-performance, triple-halide perovskite–silicon. *Journal of Perovskite Research*, 2023.

[37] Jiajia Suo, Bowen Yang, Edoardo Mosconi, Dmitry Bogachuk, Tiarnan A. S. Doherty, Kyle Frohna, Dominik J. Kubicki, Fan Fu, YeonJu Kim, Oussama Er-Raji, Tiankai Zhang, Lorenzo Baldinelli, Lukas Wagner, Ayodhya N. Tiwari, Feng Gao, Andreas Hinsch, Samuel D. Stranks, Filippo De Angelis, and Anders Hagfeldt. Multifunctional sulfonium-based treatment for perovskite solar cells with less than 1% efficiency loss over 4,500-h operational stability tests. *Nature Energy*, 9:172–183, 2024.

[38] X. Hu and F. et al. Yao. Tail states suppression via surface-modification of wide-bandgap perovskites for high-efficiency all-perovskite photovoltaic tandems. *Chemical Engineering Journal*, 2024.